



Universität  
Rostock



Institut für Innovationen



SOLENT  
UNIVERSITY  
SOUTHAMPTON



Zachodniopomorski  
Uniwersytet  
Techniczny  
w Szczecinie



# INTRODUCTION OF PROPELLER FLOW FIELD IN A DISCRETE ELEMENT SIMULATION OF BRASH ICE

MASTER THESIS

**Submitted on :** August 30, 2020

**By :** ÇİLKAYA Emre

**Student ID :** 190615X

**Address :** Atatürk Mh., Ömer Çavuş Sk., Şahinler Sitesi D-5, Değirmendere, 41950

**e-mail :** emrecilkaya@gmail.com

**Supervisor :** Prof. Lionel GENTAZ, École Centrale de Nantes

Quentin HISETTE, The Hamburg Ship Model Basin (HSVA)



*This Master Thesis has been prepared as part of the graduation of the Master in Marine Technology specialized in Hydrodynamics for Ocean Engineering from Centrale Nantes and the graduation of the double Master degree Liège University-Centrale Nantes in the EMship+ programme*



## **ACKNOWLEDGEMENT**

Firstly, I would like to thank Prof. Dr. Janou Hennig, Managing Director of The Hamburg Ship Model Basin and Dipl.-Ing. Nils Reimer, Head of Department Arctic Technology for giving me the opportunity to perform my internship and Master Thesis in The Hamburg Ship Model Basin.

Next, I would like to express my sincere appreciation and gratitude to M.Sc. Quentin for his invaluable help, continuous supervision, and his patience throughout this study. I would like to convey my sincere thanks to Thomas Klemme and Dr. -Ing. Jörn Kröger from the CFD department of the HSVA for sharing their knowledge and experience in CFD.

Finally, I am grateful to my dear older brother Kazim Onur Çilkaya for proofreading the study and improving its grammar.

## Contents

<b>List of Figures</b>	<b>vii</b>
<b>List of Tables</b>	<b>ix</b>
<b>1 Introduction</b>	<b>1</b>
1.1 Definition of Brash Ice . . . . .	2
<b>2 Performance Estimation of Ice Class Ships in Brash Ice</b>	<b>4</b>
2.1 Model Test . . . . .	4
2.2 Ice Class Rules . . . . .	6
2.3 Theoretical Formulas . . . . .	6
2.4 Numerical Simulation . . . . .	8
2.4.1 Physically Based Modelling . . . . .	8
2.4.2 Smoothed Particle Hydrodynamics (SPH) . . . . .	9
2.4.3 CFD-DEM Coupling . . . . .	9
2.5 Objectives and Goals . . . . .	15
<b>3 General Description of Initial DEM Tool</b>	<b>17</b>
3.1 Brief Definition of Discrete Element Method . . . . .	17
3.2 Brash Ice Simulation Types . . . . .	18
3.2.1 Brash Ice Creation . . . . .	18
3.2.2 Cylinder Experiment Simulation . . . . .	18
3.2.3 Brash Ice Ship Model Test Simulation . . . . .	19
3.3 Basic Structure of Brash Ice Simulation Algorithm . . . . .	20
3.3.1 Element Initialization . . . . .	21
3.3.2 Predictor . . . . .	22
3.3.3 Overlap Computation . . . . .	23
3.3.4 Force Computation . . . . .	23
3.3.5 Corrector . . . . .	25
3.3.6 Program Output . . . . .	25
3.4 Hydrodynamics Improvements on Brash Ice Simulations . . . . .	25
3.4.1 Flow Field Conversion . . . . .	25



3.4.2	Importing CFD Flow Field Into Brash Ice Simulations . . . . .	26
3.4.3	Drag Force Computation . . . . .	28
3.5	Area of Improvement . . . . .	29
<b>4</b>	<b>Flow Field Around Propeller</b>	<b>31</b>
4.1	Actuator Disk Theory . . . . .	31
4.2	Properties of the Propeller . . . . .	32
4.3	Numerical Spatial Domain . . . . .	33
4.4	Simulation Setup . . . . .	34
4.5	CFD Simulation Results . . . . .	36
4.6	Automating the Actuator Disk Simulation . . . . .	38
4.7	Flow Field Conversion . . . . .	39
<b>5</b>	<b>Further Improvements on Hydrodynamic Module</b>	<b>42</b>
5.1	Description of Improved Tool . . . . .	42
5.2	The Proof of Modified Tool . . . . .	44
5.2.1	Cylinder Simulation with Improved Tool . . . . .	45
5.3	Simulation of Model Ship Experiment . . . . .	47
5.3.1	Flow Field Around Ship . . . . .	47
5.3.2	Brash Ice Model Simulation . . . . .	52
<b>6</b>	<b>Conclusion</b>	<b>59</b>
<b>7</b>	<b>Recommendations For Future Studies</b>	<b>60</b>
	<b>References</b>	<b>61</b>

## **Declaration of Authorship**

I declare that this thesis and the work presented in it are my own and have been generated by me as the result of my own original research.

Where I have consulted the published work of others, this is always clearly attributed.

Where I have quoted from the work of others, the source is always given. With the exception of such quotations, this thesis is entirely my own work.

I have acknowledged all main sources of help.

Where the thesis is based on work done by myself jointly with others, I have made clear exactly what was done by others and what I have contributed myself.

This thesis contains no material that has been submitted previously, in whole or in part, for the award of any other academic degree or diploma.

I cede copyright of the thesis in favour of the University of Liège and École Centrale de Nantes.

**Date:** 30/08/2020

**Signature:**

A handwritten signature in black ink, appearing to be 'E. Van der...'.

## **ABSTRACT**

The decline in the ice extent in the polar region as a result of global warming transforms the polar region into an ocean that is available to navigate for vessels without ice breaking capability. As the commercial vessel traffic increases at the polar region, the investments are made on the determination of ice-going cargo vessels' performance in the brash ice channels where it navigates through. There are many methods offered such as model test experiments, mathematical models, ice-class rules, and computer simulations based on the CFD (Computational Fluid Dynamics) and DEM (Discrete Element Method) to determine the performance of such ships.

The HSVA (Hamburg Ship Model Basin) develops a tool based on the DEM to simulate the performance of a ship in brash ice. In the developed tool, the brash ice particles' motion around the ship due to the brash ice particles-ship contact forces can be visualized. The tool is also capable of importing a flow field acquired by the CFD into the software, calculating the hydrodynamic drag force of the brash ice particle, and observing the brash ice particles' movement due to a flow field.

In this study, the tool is further improved so that it allows to import multiple flow fields belonging to the propellers and the ship separately. The propeller is modelled as an actuator disk so that it calculates a volume force distributed along the actuator disk region depending on the propeller characteristics, and transfers the calculated momentum from the propeller to the fluid. The next important step is to automate the CFD propeller simulation so that it can be directly used inside the DEM tool. A command line based user interface is created taking the required parameters from the user so as to start the CFD simulation for a propeller. The necessary CFD results such as the velocity field, residual graph are automatically saved after the simulation ends without using the GUI (Graphical User Interface) of post-processing software (ParaView).

After the automation step for the flow around a propeller, the CFD simulation is performed to determine the flow around the ship. Then the brash ice model simulations with no flow field, single flow field (flow around the ship), and multiple flow fields (the ship and the propeller flow fields) are executed. The qualitative results are compared for the simulations. It is concluded that the modified tool works well; it affects the brash

ice movement around the ship, and at the propeller region. Furthermore, it also affects the number of brash ice particles interacting with the ship, and the brash ice resistance, consequently. However, it is observed that the simulation must be carried out with a large number of brash ice particles in order to make a proper visual assessment in comparison with the experimental results.

## List of Figures

1	Ship passing through brash ice channel [2]	1
2	Brash Ice [5]	3
3	Cross-section of a brash ice channel [1]	3
4	Brash ice model test at HSVA [4]	4
5	Brash ice channel after test run	5
6	Brash ice simulation performed via physics engine [8]	8
7	Particle view in SPH simulation[2]	9
8	The comparison of two different modelling approaches [9]	10
9	The velocity distribution of brash ice particles around the vessel for one-way and two-way coupling [3]	11
10	Ice injection method [10]	12
11	A ship advancing through ice-floe region [10]	12
12	Simulations done for different frictional coefficients and RPS [11]	13
13	Hull brash ice resistance for different ship speeds and brash ice densities [13]	15
14	Basic DEM flowchart [4]	17
15	Brash ice channel simulation with floating up technique	18
16	Cylinder experiment simulation [14]	19
17	Ship model simulation in brash ice (bottom view) [4]	19
18	Flowchart of DEM simulation tool [14]	20
19	An example of ship geometry to insert into DEM tool	21
20	Hydrostatic data table [16]	22
21	Contact detection modelling for brash ice simulations [4]	23
22	Grid conversion [14]	26
23	Matching process [14]	26
24	Schematic for 3-D velocity arrays [14]	27
25	Flow field and brash ice channel domains [14]	27
26	Trilinear interpolation [14]	28
27	Brash ice velocity diagram before and after inserting a flow field [14]	29
28	Normalized volume forces versus normalized radius [17]	32
29	Actuator disk	33
30	Spatial domain and its discretization	34

31	Comparison of normalized axial velocities . . . . .	36
32	Normalized axial volume force . . . . .	37
33	Convergence history for actuator disk simulation . . . . .	38
34	Actuator disk CFD simulation interface . . . . .	39
35	Comparison of actuator disk velocity fields between converted flow field and CFD flow field . . . . .	41
36	3-D velocity arrays for multiple flow fields . . . . .	43
37	Domains of multiple flow fields and brash ice . . . . .	44
38	Brash ice velocity diagram for multiple flow fields . . . . .	44
39	The configuration of the cylinder brash ice simulation for validation study .	45
40	Comparison of cylinder brash ice simulations . . . . .	46
41	Original and modified ship geometry . . . . .	48
42	Numerical domain for ship simulation. A. general view of the numerical domain; B. zoomed view near inlet boundary; C. zoomed view near the hull model; D. zoomed view near outlet boundary . . . . .	49
43	Discretized numerical domain for ship simulation. A. overall mesh; B. mesh around the ship; C. mesh around the bow; D. mesh around the stern; E. mesh around ship midsection . . . . .	50
44	Residual convergence history for flow around the ship . . . . .	51
45	Force convergence history for flow around the ship (zoomed view) . . . . .	51
46	Extracted domain for the flow field conversion simulation (red: extracted domain, green: hull, grey: entire numerical domain) . . . . .	52
47	Comparison of ship velocity fields between the converted flow field and the CFD flow field (bottom views) . . . . .	54
48	Comparison of ship velocity fields between the converted flow field and the CFD flow field (side views) . . . . .	54
49	Triangulated ship mesh used in the brash ice model simulation . . . . .	55
50	Brash ice model simulation configuration . . . . .	56
51	Comparison of ship model brash ice simulations . . . . .	57
52	Detailed comparison of the simulations (multiple flow field vs no flow field)	58
53	The underwater view of the channel behind the ship model for both exper- iment and simulation with multiple flow fields . . . . .	58

## **List of Tables**

1	Summary of acting forces [4] . . . . .	24
2	Basic characteristics of propeller . . . . .	33
3	Mesh quality of the actuator disk domain . . . . .	34
4	Boundary conditions for actuator disk simulation . . . . .	35
5	Main particulars of the model ship . . . . .	48

## 1 Introduction

As a result of the increasing effect of global warming, the ice extent in the Arctic is declining quickly. When the ice retreats, it creates open water in which the commercial shipping routes through the Arctic region become available to navigate. In addition, the discovery of large commodities such as natural gas and oil in Arctic region brings about an increase in shipping traffic in Arctic. And it leads to the requirement for accurate power prediction of an ice-going cargo vessels operating in brash ice channels which are waterways covered with relatively small-size ice rubble [1]. These vessels are not able to break the ice by themselves; however, they are ice-class ships having the capability of sailing into the brash ice channels created by ice-breaking vessels.



**Figure 1:** Ship passing through brash ice channel [2]

In the design stage of these ships, in addition to water resistance, ice resistance must also be taken into account which contributes to the total resistance of an ice-going ship substantially. Theoretical analysis, empirical formulas, numerical simulations and model testing are the most favoured methods of examining ice-ship interaction. Among the listed methods, however, a large amount of experimental data is essential for both theoretical methods and empirical formulas. Although tank testing for ice-ship interaction provides the most reliable data, it has a downside in terms of the high cost related to the ice tank and ice generation; therefore, it is not an affordable choice for most researchers [3]. Furthermore, the model tests are conducted at the advanced design stage. Therefore,



there is another method required to predict the added ice resistance, to design an efficient hull, and to detect early design flaws before undertaking an expensive model test.

With the advance of computer technologies, numerical simulation methods such as CFD and DEM are not computationally demanding as before. Thus, it is more affordable and feasible to perform such simulations to investigate the ship hull-brash ice-fluid interaction in the early design stage of an ice-going vessel.

In order to study the fluid interaction with DEM particles (brash ice particles in this case), a combined DEM-CFD approach is needed. The flow field of an advancing ship can be solved using Computational Fluid Dynamics (CFD). Afterwards, these CFD results can be further integrated into the DEM simulation to determine the contact forces arising from the ice-ice and ship-ice interaction. In this way, the hydrodynamic effect of the flow around the ship on the brash ice particles when it passes through the brash channel, as well as the contact forces occurring between the DEM particles, can be determined, and more accurate, quantitative and qualitative results can be obtained.

## **1.1 Definition of Brash Ice**

Brash ice is an accumulation of floating ice made up of fragments not more than 2m across. When the ice breaker ship navigates through the level ice, it forms a channel filled with broken ice pieces. Ice class ships without ice breaking ability follow the same route and break the previously broken ice pieces into even smaller pieces. Due to ship navigation and repeated traffic, ice pieces take shape similar to a sphere because of the rounding off the edges by colliding with passing ships [4].



**Figure 2:** Brash Ice [5]

The layer of brash ice accumulated in a regularly navigated ice channel is much thicker than the level ice sheet surrounding the channel. The cross section of the brash ice channel is presented in the following schematic.

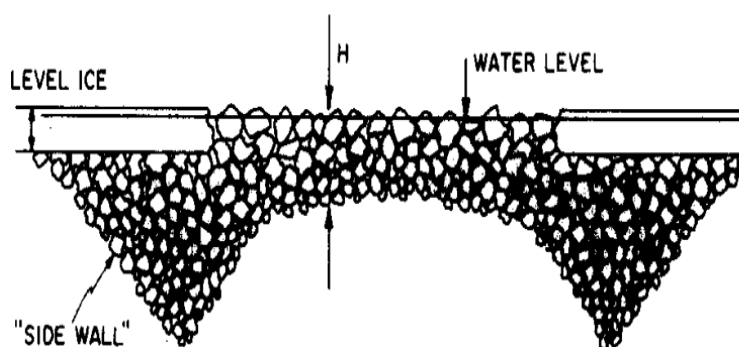


**Figure 3:** Cross-section of a brash ice channel [1]

## **2 Performance Estimation of Ice Class Ships in Brash Ice**

The performance of a ships in brash ice can be determined in various ways such as numerical simulations, model tests, ice class rules, and theoretical analysis. In this chapter, the usage of these methods found in literature is presented in different subtitles. Since the main focus of this study is predicting ship performance by performing numerical simulations, more detailed research is dedicated to that method.

### **2.1 Model Test**

There are several ice model basins exist to conduct experiments so as to determine the performance requirements of ice class ships such as the HSVA (Hamburg Ship Model Basin), Krylov, and Aker Arctic.

At the HSVA, the brash ice model tests are conducted to investigate the performance of ships passing through the brash ice channel. After the preparation of the brash ice channel according to the HSVA's standard model ice procedure, the model test is carried out by pulling the ship model by the carriage at a constant speed. The towing force is measured by a load cell mounted at the bow of the model. During a test run, the rotational speed of the propeller is gradually changed four times to use the channel length optimally. At the lowest RPM, the propulsive thrust approaches to the zero thrust condition. On the other hand, at the highest RPM, the propulsive thrust increases above the self propulsion point; as a result, the model is pushing the carriage.



**Figure 4:** Brash ice model test at HSVA [4]

In accordance with the HSVA's standard, the following parameters can be determined in the towed propulsion test;

- Total (towing) resistance in ice
- Developed thrust at self propulsion
- Delivered power at self propulsion
- Propeller efficiency behind the model in ice
- Thrust deduction factor in ice

Linear relation between the towing force and developed thrust can be established after assuming that the thrust deduction factor is independent from propeller RPM and thrust. Then, the towing force which is equivalent to the total resistance in the ice can be attained when the propeller thrust is vanishing. Similarly, using this linear relation, propeller thrust can also be determined at the self propulsion point when the towed force is vanishing. Another regression analysis can be established between delivered power and developed thrust. Thereby, the delivered power can then be determined for developed thrust at the self propulsion point.

The results obtained from the test can also be used for visual assessment in comparison with simulation results. The following photo is taken after the towing test run of an ice-going ship model.

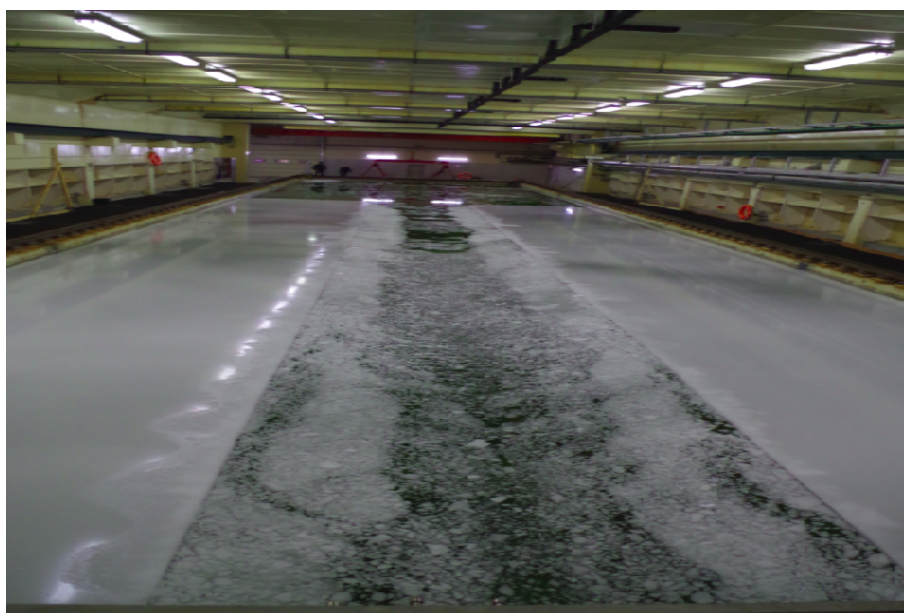


**Figure 5:** Brash ice channel after test run

## 2.2 Ice Class Rules

According to the FSICR (Finnish-Swedish Ice Class Rule), the engine output of a ship operating in brash ice should not be less than determined by the following formula.

$$P = K_e \frac{(R_{CH}/1000)^{\frac{3}{2}}}{D_p} [kW] \quad (1)$$

where,

- $K_C$  is propeller related constant factor
- $D_p$  is propeller diameter
- $R_{BC}$  is the resistance in Newton of the ship in a channel with brash ice. It is calculated according to the formula provided by FSICR [6].

The above equation is valid for the ships entitled to ice class IA Super (ships operating without the assistance of an ice breakers), and the lower class ships requiring ice-breaker assistance IA, IB, and IC [6].

## 2.3 Theoretical Formulas

There are many of formulas that have been proposed by researchers to calculate the ice resistance of a ship sailing through channel clogged with brash ice. Dobrodeev et al. attempted to develop a theoretical model devoted to performance of ship in brash ice [7]. They compare the calculation results obtained through the proposed model with experimental data from ice model basin located at Krylov State Research Center. The general expression of the formula to estimate the brash ice resistance of the ship is given as follows:

$$\begin{aligned} R_{BC} = & \Delta\rho(1-n)gTh_{BC} \frac{B}{2\sin\alpha_0} \left[ 1 + \frac{1}{\sin\alpha_0} \left( 1 - \frac{2T}{B} \right) \right] + \\ & \rho_I(1-n) \frac{B}{2\sin\alpha_0} h_{BC} V_s^2 \left( \frac{1}{\sin\alpha_0} + \frac{1}{\sin\varphi_0} \right)^2 + \\ & f_I \Delta\rho(1-n)gh_{BC} \frac{B-2T}{\sin\alpha_0} \left[ L_{PM} - \frac{V_{bott}\sin\alpha_0}{B-2T} + \frac{T\cos\theta}{tg\varphi_0} \right] + \\ & 2f_I \Delta\rho(1-n)gS_{PM}L_{PM} \frac{\sin\psi\cos\gamma}{\cos(\psi+\gamma)} \end{aligned} \quad (2)$$

where,

- $\Delta\rho$ : ice/water density difference
- $n$ : brash ice porosity
- $T$ : ship draught
- $B$ : ship beam on design waterline
- $h_{BC}$ : thickness of brash ice ahead of ship
- $\alpha_0$ : angle of waterline slope at the bow with respect to the centerplane
- $\rho_I$ : ice density
- $\varphi_0$ : angle of stem
- $f_I$ : coefficient of ice friction against hull plating
- $L_{PM}$ : Length of ice pile by ship's side
- $V_{bott}$ : volume of brash ice thrown from ship's bottom to one side
- $S_{PM}$ : cross-section area of ice pile by ship's side
- $S_{PM}$ : cross-section area of ice pile by ship's side
- $R_{BC}$ : resistance of brash ice in channel

This formula allows to define the brash ice resistance in terms of ship's main dimensions, bow shape, and brash ice properties. In the study, the total brash ice resistance is split into the following components;

- resistance arises from brash ice accumulation by the ship hull over a distance equal to the ship draught
- momentum resistance due to instant velocity of brash ice particles transmitted by the hull
- resistance due to the friction of brash ice particles against ship's bow, stern, and bottom
- brash ice frictional resistance against ship's sides.

As a result of the study, it is found that the total ice resistance estimated by the developed mathematical model is in good agreement with experimental results [7].

## 2.4 Numerical Simulation

In this section, the literature findings related to predicting ice-class ship performance in brash ice using numerical simulations are presented. Depending on the numerical method performed, the findings are explained under several subsections.

### 2.4.1 Physically Based Modelling

Physically based modelling, which is commonly used in computer graphics animation and computer games, is an approach to simulate the force interaction between countless rigid solid particles that are independent from each other [8]. The study of Konno A. et al. [8] can be mentioned as an example from the literature for the application of this concept on the performance prediction of a ship in brash ice. In the study, this method is utilized to conduct numerical simulations of a model ship test in brash ice channel with different advance speeds, and the results are compared with the experimental data. The fluid force exerted on an ice piece is modelled using the following virtual force formula.

$$\vec{F} = -C_D A \cdot \frac{1}{2} \rho |\vec{v}| \vec{v} \quad (3)$$

where,

- $C_D$  is the coefficient of drag
- $A$  is the ice piece projection area
- $\rho$  is the water density
- and  $v$  is the velocity of an ice particle

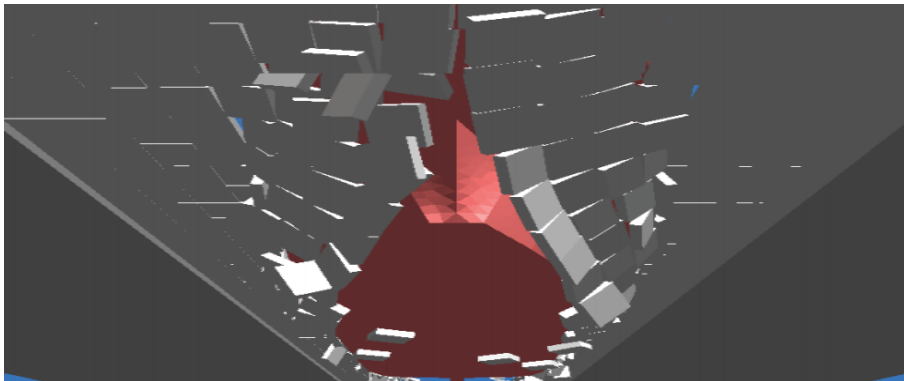


**Figure 6:** Brash ice simulation performed via physics engine [8]

The study concludes that the simulation results are in good agreement with the experiment; although, the the tendency of relationship between carriage velocity and resistance are found to be different between numerical simulation and the experiments. In addition, nonphysical adhesion of ice pieces on the ship hull as well as unrealistic oscillations of the ship are also noticed; making further studies a requirement [8].

#### **2.4.2 Smoothed Particle Hydrodynamics (SPH)**

Montenegro Cabrera utilized smoothed particle hydrodynamics (SPH) in order to perform brash ice simulation in his master thesis [2]. The single phase granular flow model is solved with SPH method and the results are compared with the experiment. It is asserted that this method would be a good candidate to model the brash ice behaviour. The study regards the qualitative results of the simulation as a good first approach to observe the behaviour of granular brash ice particles. However, quantitative validation is a requirement for final conclusion [2].

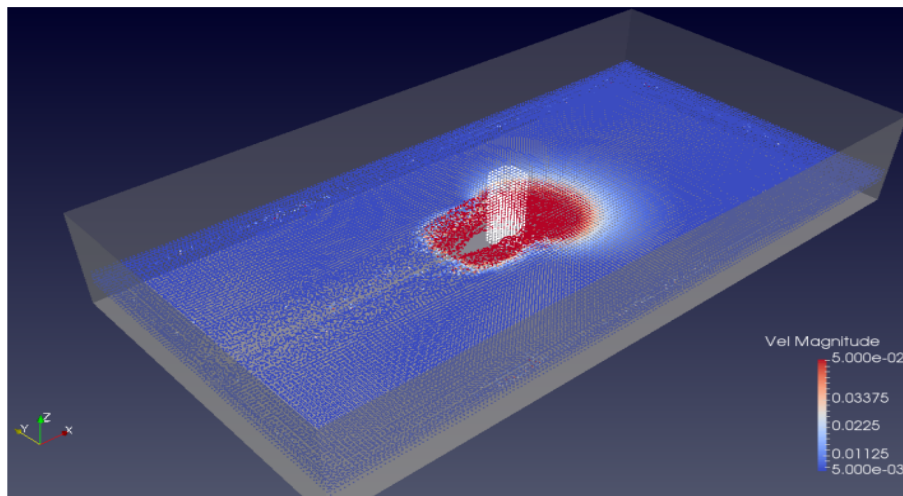


**Figure 7:** Particle view in SPH simulation[2]

#### **2.4.3 CFD-DEM Coupling**

Philipp Mucha proposed a method for the simulation of ships passing through brash ice by coupling Computational Fluid Dynamics (CFD) to the Discrete Element Method (DEM) [9]. The aim of the study was to produce a better simulation approach for estimating resistance, propulsion, and local flow field.

The CFD is modelled based on Reynolds-averaged Navier-Stokes (RANS) equations together with Volume of Fluid (VOF) for modelling the free surface. Then, DEM is imple-



mented to simulate ship-ice interaction. With this coupling approach, the effect of the flow field induced by the advancing ship on the DEM particles, as well as the modification of flow field due to the movement of the ice particles can be taken into account. In addition, propulsion analysis is also performed to observe the presence of ice in the local inflow of the propeller. The difficulty of the coupling approach lies in coupling the two phases: Eulerian phase of air and water to the Lagrangian phase of ice.

There were two methods employed such that upstream injection method where the ship is not moving and DEM particles are injected into the flow field, and the ship is moving through DEM particles. The first one gives more realistic results by collective behaviour of ice particles on the flow disturbed by advancing ship; on the other hand, it is computationally demanding compared to injection method. The visual comparison between two method is given in the following figure.

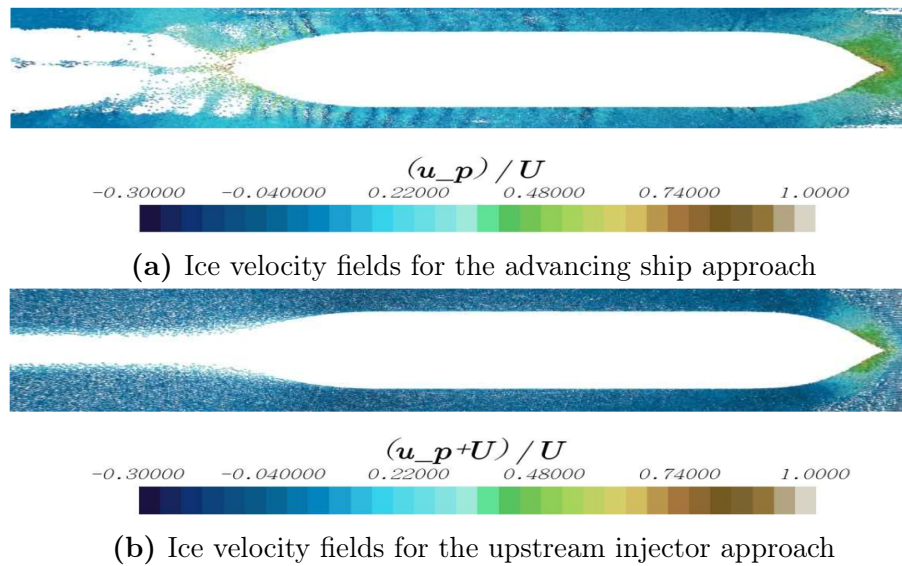


**Figure 8:** The comparison of two different modelling approaches [9]

Similar study was conducted by Luo et al. so as to perform a simulation of an ice-strengthened bulk carrier in brash ice by performing DEM-CFD coupling [3] with particle injection method. Again, ship-water and ship-ice interactions are constructed under Euler and Lagrangian framework, respectively. The comparison of the results between one-way coupling and two-way coupling computational schemes is displayed in the following figure.

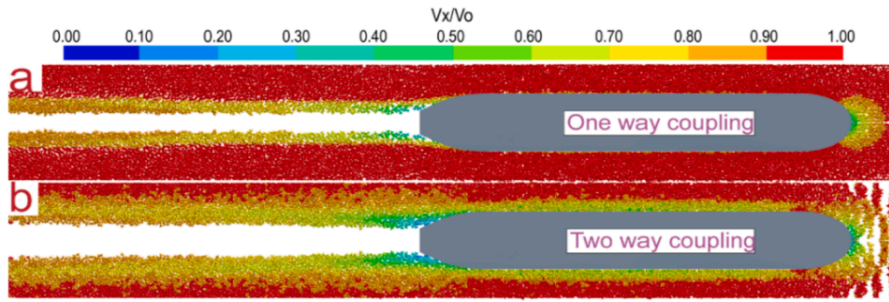
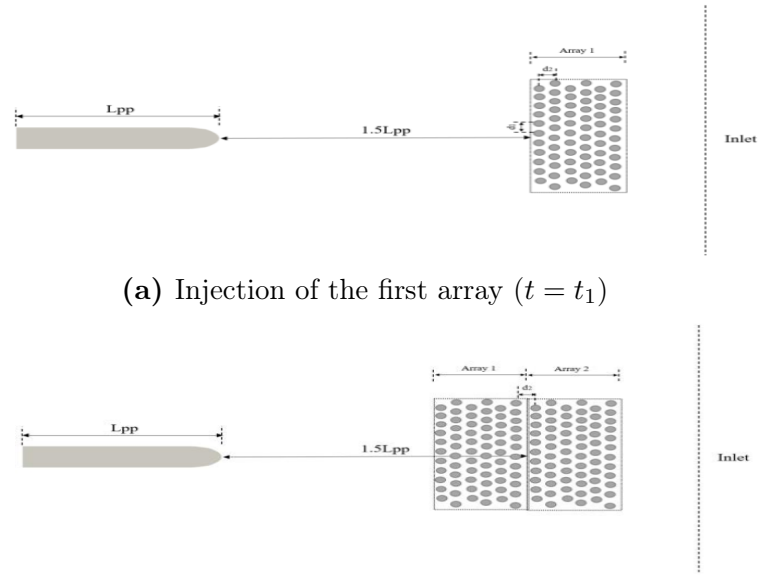


**Figure 9:** The velocity distribution of brash ice particles around the vessel for one-way and two-way coupling [3]

Both methods transfer the momentum and energy of the fluid calculated by CFD onto the DEM particles. The difference between one-way and two-way coupling is that in case of one-way coupling, ice movements in the fluid does not create any disturbance in the flow field; the interaction between ice particles and the fluid is ignored. In the two way coupling, however, this interaction is considered.

It is concluded that two-way coupling gives more accurate and realistic results when compared to reference data from the model test. On the other hand, two-way coupling method requires more computational power than one-way coupling. Furthermore, one-way coupling is recommended for low speed simulations where the flow disturbance arising from fluid-brash ice interaction is not significant [3].

Furthermore, Huang et al. performed CFD-DEM coupled simulations to investigate hydrodynamics of ship advancing in floating ice floes [10]. In the study, an innovative approach was used for injecting the DEM particles (ice floes) such that the ice floes are injected one another without disturbing the stability of the fluid domain near the ship; thus ship enters continuous ice-floe area with minimal domain size achieved. It is stated that this approach can significantly decrease the computational burden. First, the CFD simulation was run for a certain time to permit the fluid domain to attain steady-state, then an ice floe array is injected near the inlet.



(a) Injection of the first array ( $t = t_1$ )

(b) Injection of the second array ( $t = t_{inject}$ )

**Figure 10:** Ice injection method [10]

The total resistance is calculated as the combination of ice resistance and water resistance. Moreover, comparison was also made with the experimental data validating that the simulations are able to estimate accurately the ship resistance.

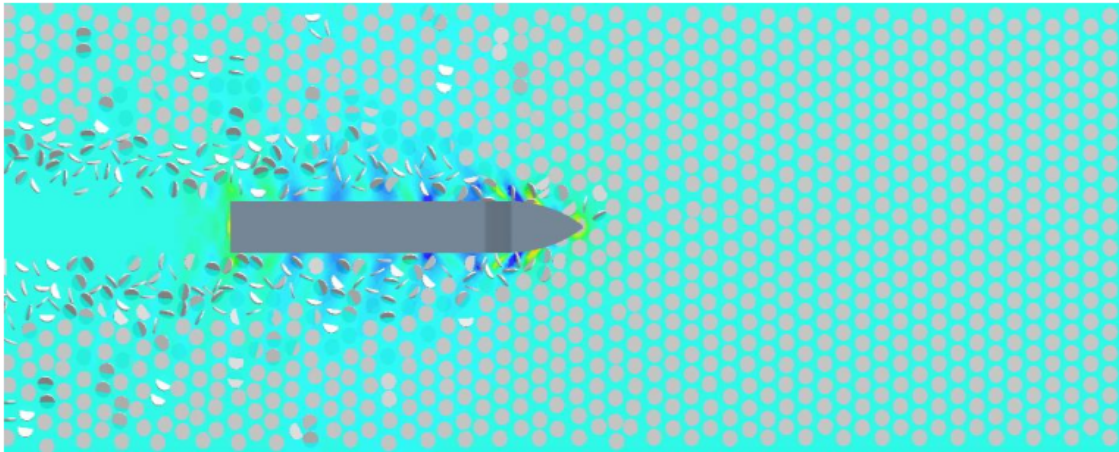


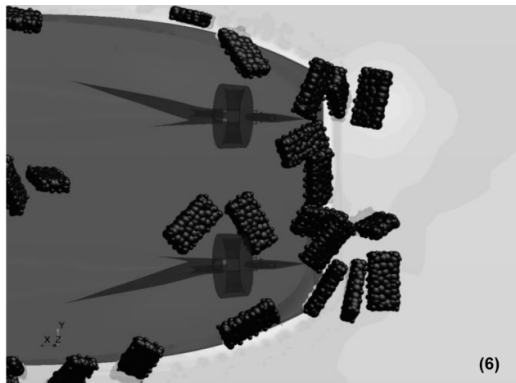
**Figure 11:** A ship advancing through ice-floe region [10]

The study demonstrates that ship-generated waves reduce the ice resistance and ice-added resistance is more critical at low ship speed [10].

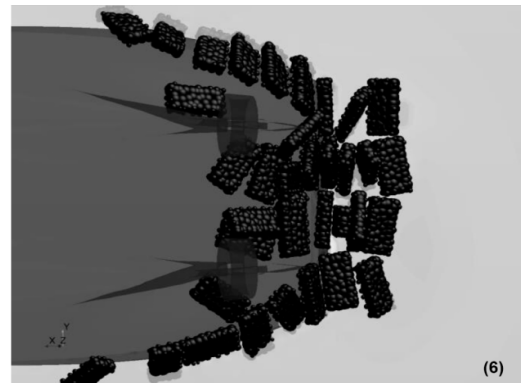
Another study by Dong Cheol Seo and Robert Pallard is performed to demonstrate the interaction between ice particles and the ship during its astern operation by making use of two-way CFD-DEM coupling approach [11]. The main focus of the study is to observe ship-ice interaction around the stern area of the ship where the flow field becomes very

complex due to the propeller and the appendages. In order to reduce the computational burden, the propeller is modelled as virtual disc.

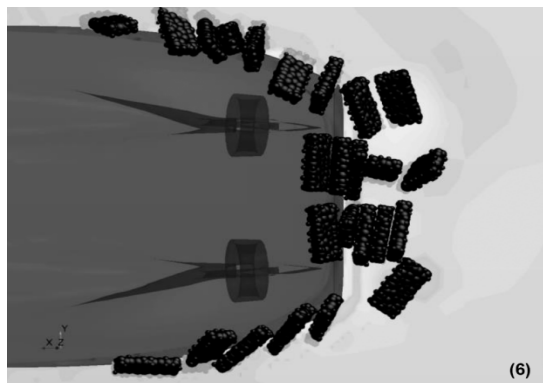
CFD analysis is first run until achieving steady-state condition, then the several hexahedral shape ice pieces are injected into the steady-state flow sequentially. Simulations are run for different RPS (rotation per second) and frictional coefficient. The visual results of the simulations are presented in the following figures.



(a) Simulations done for 13 RPS and 0.05 Frictional Coefficient



(b) Simulations done for 13 RPS and 0.3 Frictional Coefficient



(c) Simulations done for 0 RPS and 0.3 Frictional Coefficient

**Figure 12:** Simulations done for different frictional coefficients and RPS [11]

The paper concludes that the hydrodynamic interaction between propeller and ice particles can affect the location of the ice accumulation. It is also stated that the use of virtual disc model is computationally more efficient than using a moving reference frame method (MRF) with propeller geometry. Moreover, it is identified that the results obtained can only give a qualitative information that relies on visual images meaning that CFD-DEM method requires rigorous validation. For more accurate result, it is suggested that propeller blade-ice contact and particle trajectory should also be studied for more

dependable results. Finally, it is concluded that CFD-DEM coupling method should be optimized in terms of domain size and number of ice particles used in the simulation; since, it is computationally demanding [11].

In Erik Vroegrijk's paper [12] investigations are purely dedicated to validate full scale CFD-DEM coupling simulations by measured data. In the paper, the measured data is drawn from full scale measurements (e.g hull-ice interaction, propeller rpm etc.) of on-board a double-ended ferry. In the study, first the CFD simulation is performed until reaching converged flow field. Then DEM particles are injected into the numerical domain. In the paper the propeller action is explicitly modelled with the use of a moving reference frame (MRF) instead of using virtual disc as it is done by Dong Cheol Seo and Robert Pallard [11]. One-way CFD-DEM coupling is used in the study.

In the paper the vessel is being over-propelled to match experimental condition; in other words, propeller produces more thrust than is needed based on the open water resistance and thrust deduction. It is stated that the excess thrust should be equal to difference between total produced thrust and required open water propulsion thrust. Then the study claims that the excess thrust and added resistance due to brash ice should be equivalent. The paper concludes that the method used is not validated properly due to lack of reliable, detailed data [12].

In 2018, Wang et al. conducted CFD-DEM simulations for different speeds of a vessel and different brash ice densities so as to reveal the interaction between a hull and brash ice [13]. It is concluded in the paper that brash ice resistance increases with the increase of the ship speed; however, when the speed increases to a certain value, the brash ice resistance tends to reduce due to the wave-making around the hull which causes a repulsive effect on the surrounding brash ice; reducing the possibility of contact and collision between the hull and brash ice [13].

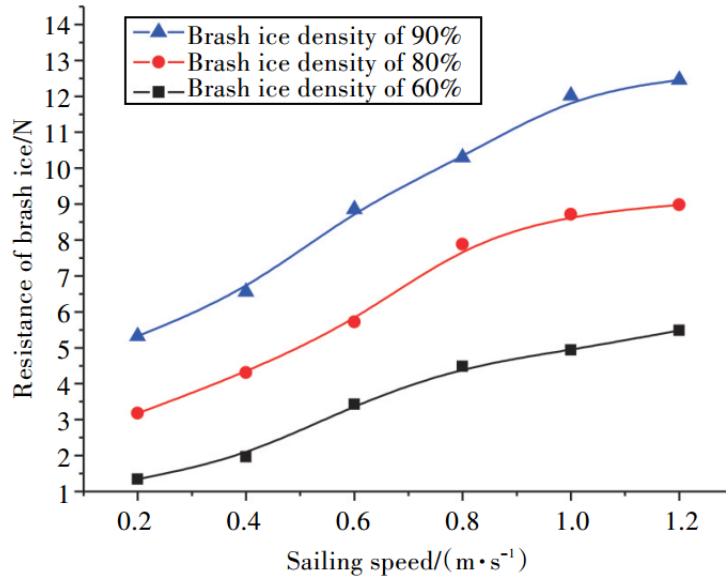


**Figure 13:** Hull brash ice resistance for different ship speeds and brash ice densities [13]

## 2.5 Objectives and Goals

HSVA has been developing a numerical simulation tool written in FORTRAN language and based on Discrete Element Method (DEM) to estimate the performance of a ship passing through numerical brash ice channel. The tool is capable of creating artificial brash ice channel, then performing a simulation for ship model test. This was introduced in the master thesis of Malith Prasanna [4].

In the ship model simulation, however, the hydrodynamic effect of ship on the ice particles were not taken into account, only the contact forces between the particles and the ship were considered. Sophie Demmin, in her thesis, introduced the hydrodynamic effect into the tool in order to improve motion of simulated brash ice particles [14]. She, first executed a steady-multiphase CFD calculation to determine the flow around cylinder, then developed a module to convert the unstructured CFD mesh into a structural rectangular grid to reduce the computation time. Subsequently, she imported the converted CFD flow field into the brash ice simulation for the cylinder experiment and tested. The flow field is coupled with the cylinder movement such that it is advancing through the channel along with the cylinder. Finally, the water velocity is added to every brash ice particle's relative water velocity, and the resultant velocity is inserted into the drag force calculation. According to the findings of Sophie Demmin, the simulation tool gives promising results in terms of visual observations of the brash ice movements around the cylinder [14].

The latest simulation tool modified by Sophie Demmin allows to insert only one flow field into the simulation. In order to improve the accuracy of the simulations, the tool must be further improved. The one of the aim of this study is to modify the brash ice simulation tool such that it will allow for insertion of multiple flow fields into the simulation. For this purpose, the steady-state CFD simulations will be performed for actuator disk and ship separately, then flow field conversion will be employed so as to simplify the CFD results for DEM calculations (brash ice model ship simulation). The another goal is here to develop a module to run the CFD simulations of an actuator disk and introduce it into the simulation. In other words, the actuator disk simulation case created via OpenFOAM will be directly run in the DEM tool in an automated way. After that, the hydrodynamic module of the tool will be modified to receive multiple flow fields inside the model ship simulation. Finally, qualitative and quantitative comparisons will be made between the simulations to validate the adapted tool.

### 3 General Description of Initial DEM Tool

In this section, the initial brash ice simulation tool in development at HSVA is introduced in terms of its functionalities, capabilities, algorithm description and set-up. After describing the initial tool, the area of improvement will be discussed .

#### 3.1 Brief Definition of Discrete Element Method

The discrete element method (DEM), also called distinct element method, is a numerical tool that computes the mechanical behaviour of numerous independent particles in interaction with each other [15]. The basic principles of the method are the identification of particle collisions and calculation of the contact forces. The particles are numerically represented by several attributes such as location, size shape, mechanical properties, and initial velocity. Furthermore, the particles are subjected to gravity and buoyancy forces.

The simulations are performed in time domain and the contact forces for colliding particles are calculated for every time step. The particles' acceleration, velocity, and displacement are determined by using Newton's equations of motion. The basic structure of DEM algorithm that applies regardless of the type of the applications with different material is given in the following flowchart [4].

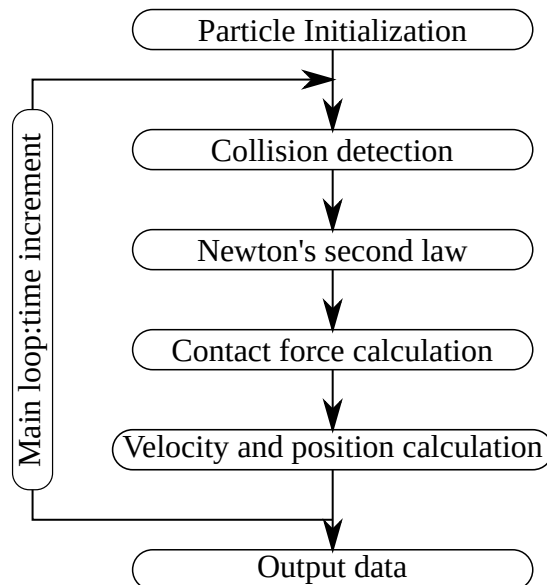


**Figure 14:** Basic DEM flowchart [4]



## 3.2 Brash Ice Simulation Types

In this section, the numerical brash ice simulation tool that exists at HSVA is described. The tool has been developed in model scale to carry out direct validation with the model test experiment. Thus, it can be considered as a numerical ice tank [4]. The brash ice simulation tool allows to perform three types of simulations;

- Brash ice creation
- Cylinder experiment simulation
- Ship model test simulation

### 3.2.1 Brash Ice Creation

The brash ice creation is base simulation type in which the numerical ice tank is generated and saved to be used in further simulations such as cylinder test or ship model test. The input parameters given by user are channel length, width, brash ice thickness, and porosity, After that, the code produces spherical ice particles based on a pre-programmed size distribution algorithm and positions them in a 3D domain below the waterline. The maximum initial speed is also assigned to every brash ice particles. Later on, the particles float up to the free surface owing to their buoyancy and form the channel. Afterwards, the channel created can be saved and used for subsequent simulations such as cylinder experiment or ship model test [4].

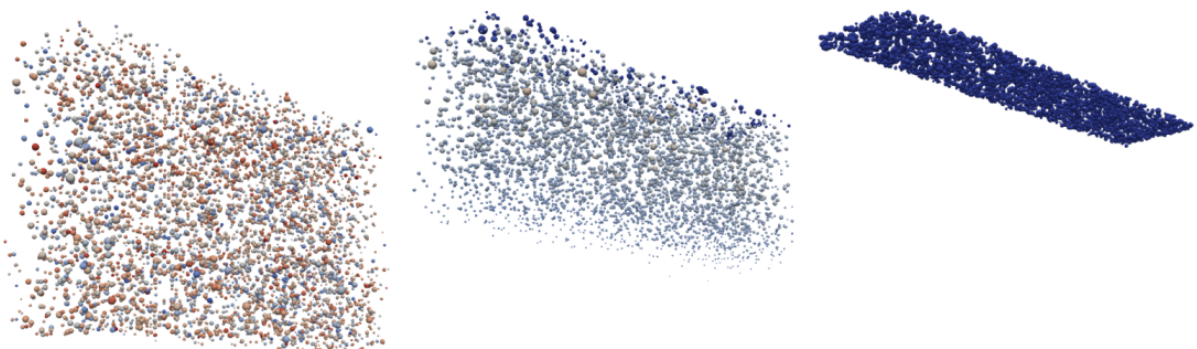


**Figure 15:** Brash ice channel simulation with floating up technique

### 3.2.2 Cylinder Experiment Simulation

Another option is to simulate a cylinder experiment on a numerical brash ice channel. Meshed 3D model of a cylinder and created brash ice channel are the inputs for this option.

This option is used as a reference test at HSVA in order to make comparison between different ice channels and validate their properties, as well as calibrating simulation results [4]. The following figure exhibits the cylinder experiment simulation where the particles are colored according to their velocity magnitude.

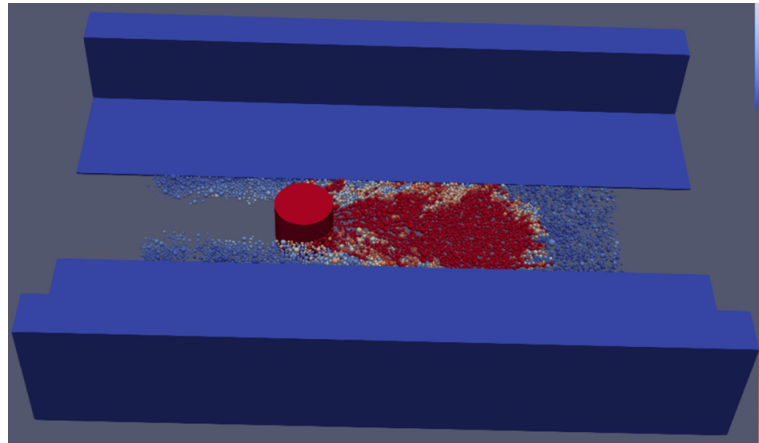


**Figure 16:** Cylinder experiment simulation [14]

### **3.2.3 Brash Ice Ship Model Test Simulation**

The final option is self-propelled ship model test simulation in brash ice. 3D meshed model of the ship, the created brash ice channel, propeller curve, and the model's open water resistance are entered as inputs to the simulation. The main purpose of the model test simulation is to determine propeller thrust for full scale engine selection, in addition to visualize ice particles flowing around the ship. It is an valuable asset to visualize ice accumulation near the stern region along with the propeller-brash ice interaction so as to determine possible design flaws at the early design stage of a vessel.

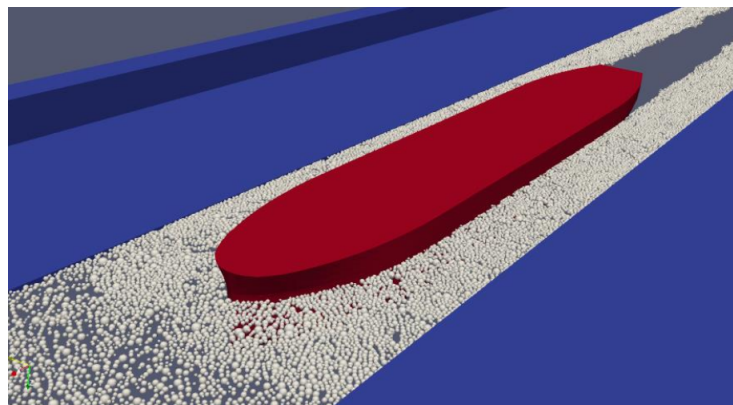


**Figure 17:** Ship model simulation in brash ice (bottom view) [4]

### 3.3 Basic Structure of Brash Ice Simulation Algorithm

The basic flowchart of a DEM software was presented in figure-14. In order for simulating ship-brash ice interactions, more sophisticated algorithm is essential. The existing brash ice simulation algorithm developed at HSVA is outlined in the following flowchart with additional steps to calculate ship dynamics and provide graphical outputs [4].

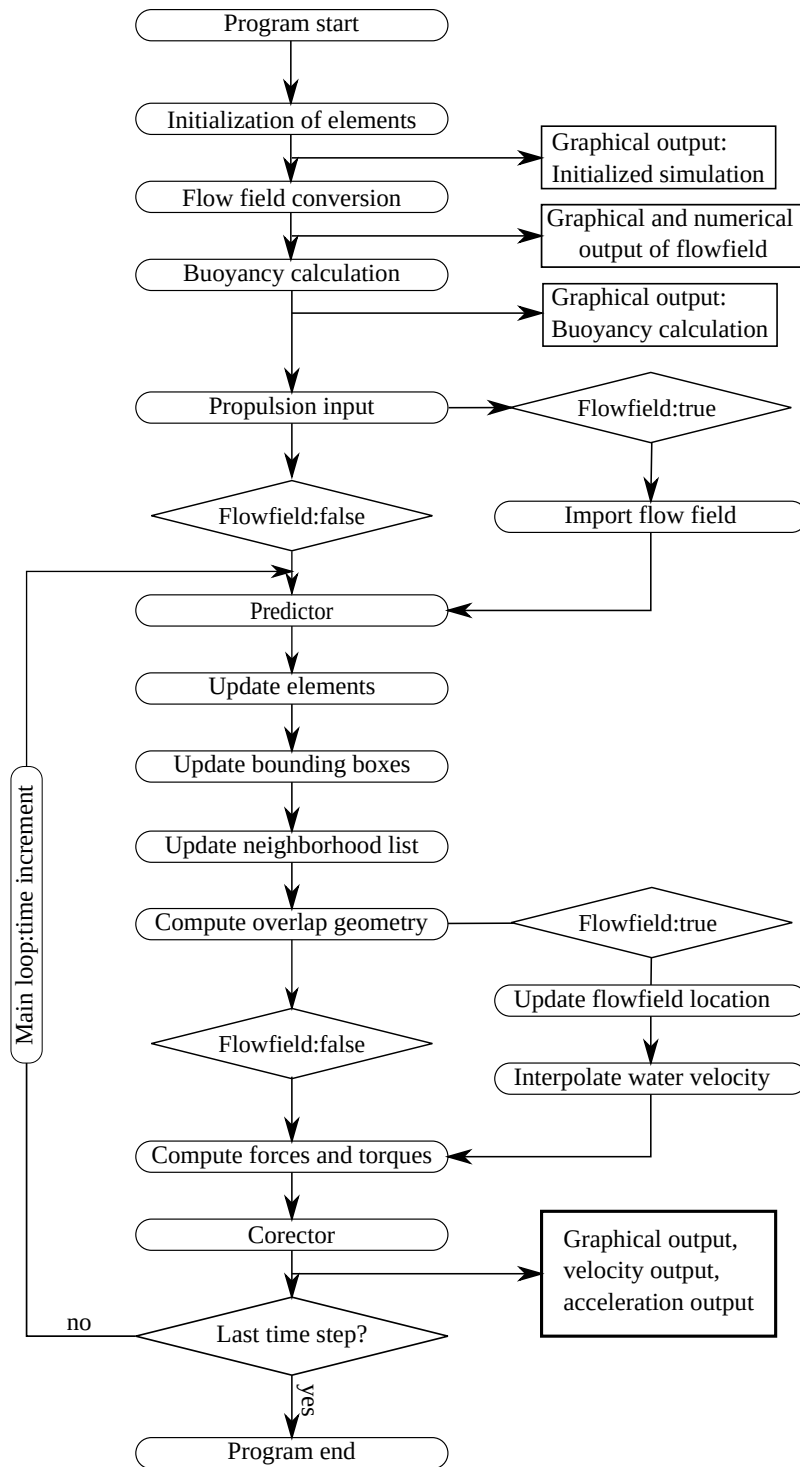


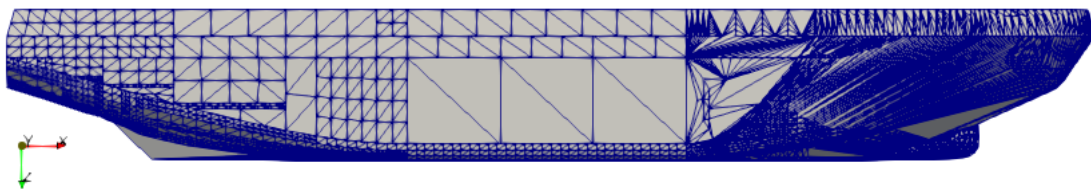
Figure 18: Flowchart of DEM simulation tool [14]

In the following sections, each steps in the flowchart (figure-18) will be explained. Since most of the steps are not modified in the context of this thesis, the steps will be explained briefly. The content of section-3.3 is mainly summary of chapter-5 and chapter-10 of Malith Prasanna's master thesis [4]. Furthermore, hydrodynamic contributions (grid conversion, update flow field location, and interpolate flow field location) to the code which were introduced by Sophie Demmin [14] will also be described at the end of this section; since, the code will be further improved on that area.

### **3.3.1 Element Initialization**

The correctness of the ultimate results is strongly linked to the accurate modelling of brash ice medium where the ship is sailing through. The brash ice particles are modelled as sphere in the code in order to simplify the simulations. This assumption is supported by stating that the full scale brash ice pieces have roundish shapes when ships sail through the channel over and over again, rounding off the edge of the ice particles.

At the initialization step, the numerical modelling of the structure is also carried out. A triangulated surface mesh is generated and inserted into the program as an .obj file. Due to the fact that the contact detection algorithm only works with convex shapes, a non-convex ship hull must be split into several convex structures and .obj files for every sub structure are inserted into the code.



(a) Triangulated mesh of a ship



(b) Ship with several sub structures

**Figure 19:** An example of ship geometry to insert into DEM tool

#### **3.3.1.1 Buoyancy Calculation**

When the ship passes through the numerical channel, its draft, trim, and heel change every

time step due to the ice force acting on the hull. Since it is computationally not efficient to run hydrostatic calculations every time step, a 3D hydrostatic table is calculated using gift wrapping algorithm - to calculate underwater section areas - and Simpson's rule - to integrate the section areas along the ship length to find underwater volume- including the ship's displacement for every cases of draft, trim, and heel before the initialisation of the main loop.

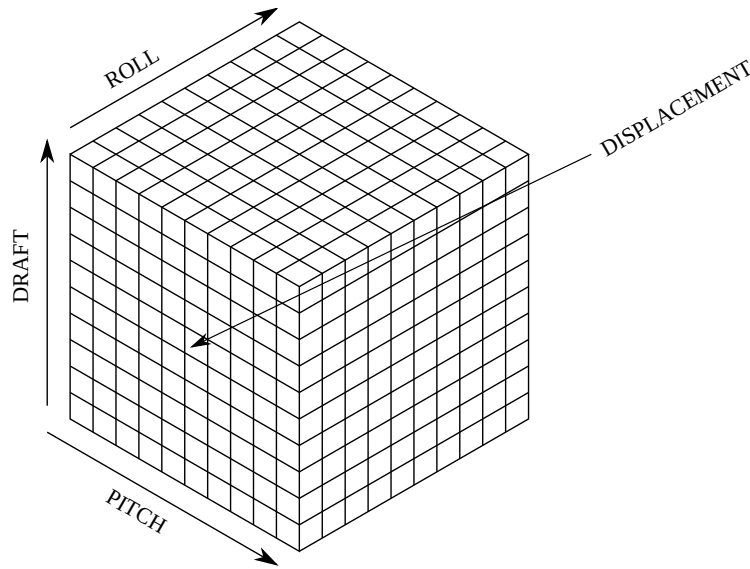


**Figure 20:** Hydrostatic data table [16]

### 3.3.1.2 Propulsion Input

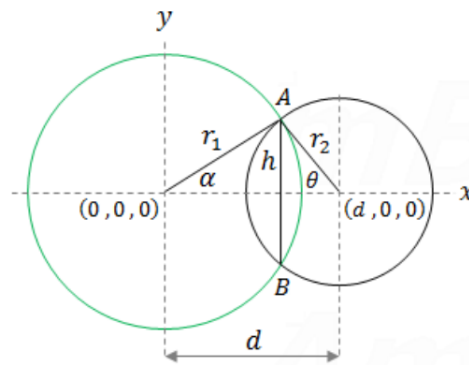
So as to calculate the propeller thrust, open water propeller characteristics are given as input to the code in the form of .csv file.

### 3.3.2 Predictor

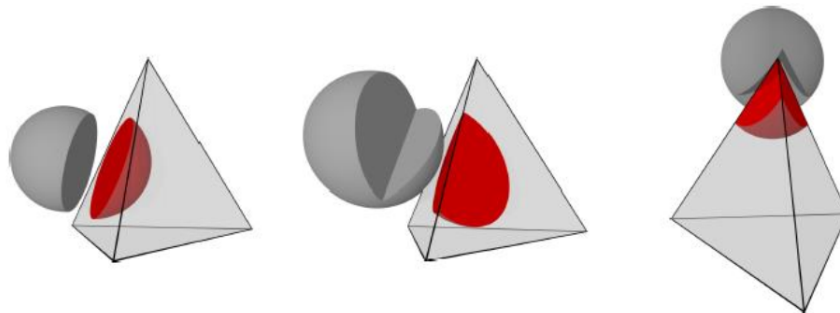
In this step, the time integration is carried out to determine velocity and the position of the ship. Therefore, implicit downwind scheme is performed for temporal discretization of dynamic equations. After that, Gear's predictor-corrector algorithm is used to solve the equations numerically. The algorithm splits into two part; first part is related to prediction of physical quantities in next time step using numerical scheme; after that, this is followed by corrector step in which the error occurring in predictor step due to the contact update is compensated.

### 3.3.3 Overlap Computation

Overlap computation algorithm scans for possible overlap between two elements. To be computationally efficient, the algorithm first detects the possible overlaps between particles by creating a bounding box surrounding the element according to its maximum dimensions. In case of an overlap of bounding boxes, these two elements are placed into possible overlap pairs list; afterwards, the contact detection algorithm checks for an overlap between elements. If the overlap occurs between two element the algorithm computes the amount of volume at the interface, and accordingly contact forces acting between two elements. There are two kinds of contact algorithm used by the tool for the brash ice simulations: ice-ice and ice-structure contact detection algorithms.



(a) Modelling of ice-ice overlap



(b) Modelling of ice-structure overlap

**Figure 21:** Contact detection modelling for brash ice simulations [4]

### 3.3.4 Force Computation

In order for implementing the dynamic equation on DEM, all the forces acting on the elements must be computed. Forces acting on an element differ in accordance with its position and interaction with other elements. The summary of the acting forces taken into account is provided in table-1.

Force	Interacting Elements	Direction of Force	Force Type
Elastic	Ice/Structure	Normal to interface of contact area	Contact
Normal damping	Ice/Structure	Normal to interface of contact area	Contact
Friction	Ice/Structure	Tangential to interface of contact area	Contact
Dissipation	Ice/Structure	Tangential to interface of contact area	Contact
Cohesion	Ice	Normal to interface of contact area	Contact
Viscous drag	Ice	Tangential to velocity vector	External
Buoyancy	Ice/Structure	Vertically downward	External
Gravity	Ice/Structure	Vertically upward	External
Propeller thrust	Ship	Horizontal in direction of ship movement	External
Open water resistance	Ship	Horizontal to opposite direction of ship movement	External

**Table 1:** Summary of acting forces [4]

The forces listed above are split into two types: contact and external forces. The external forces do not originate from element interaction unlike the contact forces. The total force acting on each particle is calculated as the sum of all forces acting on the particle. However, the forces such as propeller thrust and open water resistance force are not acting on the particles. The total force is represented by the following equation.

$$F_{total} = f_g + f_b + f_d + \sum f_{contact} \quad (4)$$

where,

- $F_{total}$ : resultant force
- $f_b$ : buoyancy force
- $f_g$ : gravitational force
- $f_d$ : drag force
- $f_{contact}$ : resultant contact force that relates to each contact the particle has with other elements

### **3.3.5 Corrector**

After computing all the forces, equation of motion can be implemented for the elements. Newton's second law of motion is employed to determine translational motion.

$$F_{total} = m\ddot{x} \quad (5)$$

where,  $F_{total}$ : the resultant force found earlier (section-3.3.4),  $m$ : mass of an element, and  $\ddot{x}$ : element acceleration. Euler's equations describing the rotational motion is applied to determine rotational movements.

$$\tau = I\omega \quad (6)$$

where,  $\tau$ :angular momentum,  $I$ :inertial tensor, and  $\omega$ :angular velocity. Then, corrector step is employed so as to solve the translational and rotational motion after applying time integration.

### **3.3.6 Program Output**

There are two types of output provided by the code: numerical, and graphical output. As for the numerical output, the total kinetic energy of the system is recorded for each time step. Furthermore, resulting brash ice channel is saved together with its position, orientation, and speed of all elements in `.txt` format to be used in further simulations such as ship model, and cylinder simulations.

Structure's positions and velocities are saved at user-defined frequency in order to create the graphical output in `.vtk` format. Also, structure's (ship or cylinder) acceleration and forces are output by the simulation at each time step.

## **3.4 Hydrodynamics Improvements on Brash Ice Simulations**

In this section, hydrodynamic improvements on the code introduced by Sophie Demmin [14] will be discussed briefly.

### **3.4.1 Flow Field Conversion**

Flow field obtained through a CFD calculation can not be imported into the DEM brash ice simulations directly. The velocity values (from CFD) at the eight nodes that surrounds



the brash ice particle are interpolated at the location of brash ice particles in order to determine the water velocity imposed on them. However, when the CFD mesh is unstructured with triangular cells, it makes the interpolation process complicated due to the irregular connectivity of the cells as well as complex neighborhood relations between the cells. Therefore, simplification of CFD grid is required by converting the unstructured grid data into rectangular structured grid. The following figure exemplifies conversion from an unstructured into a structured grid by generating a node for every coordinate combination.

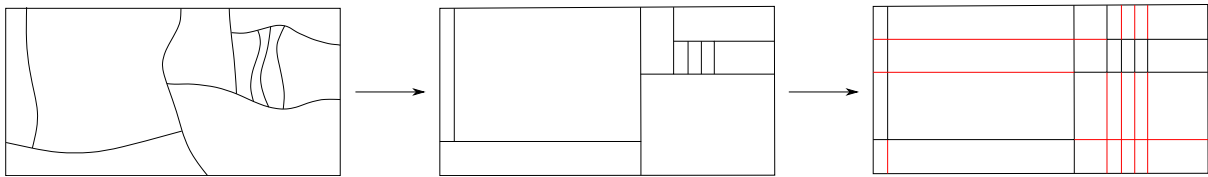


**Figure 22:** Grid conversion [14]

After creating the structured grid, the list of nodes in the unstructured grid are searched so as to find a match within the predefined tolerance value. The tolerance value is represented as green circle in the figure-23. In case if there is any node drops inside the tolerance value (green circle), the information from that node is transferred to the nearest structured grid. This is called as a match (found node) [14]. The larger the tolerance value, the more matches can be found. Finally, the missing nodes (displayed as blue cross in figure-23) containing velocity information in the structured mesh is found by interpolation. The flow field conversion introduces a separate simulation type in the tool and outputs the simplified flow field numerically and graphically.

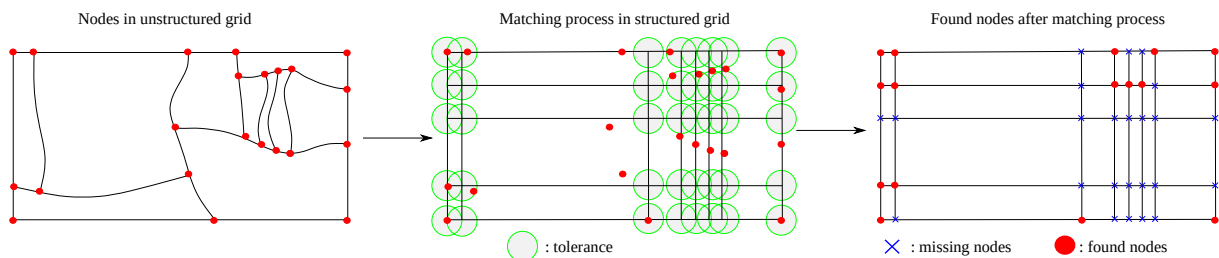


**Figure 23:** Matching process [14]

### 3.4.2 Importing CFD Flow Field Into Brash Ice Simulations

The simplified flow field that was output by flow field conversion simulation is imported into the code. The coordinate files are separately read to 1D arrays, and the velocity

files are read into 3D arrays to be further used in the following calculations regarding relocating the flow field per time step, and interpolating the velocity data at the nodes to find the velocity at the brush ice particle location every time step. The illustration of velocity arrays is shown below.

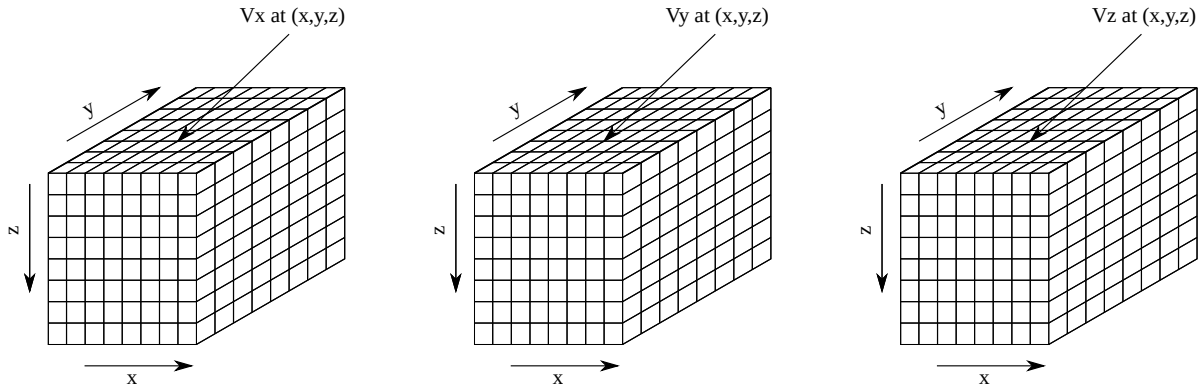


Figure 24: Schematic for 3-D velocity arrays [14]

As for the relocation of the flow field, The structure's location is added to the coordinate arrays of flow field at every time step. The schematic is presented below showing the flow field and the structure moving through the brush ice channel.

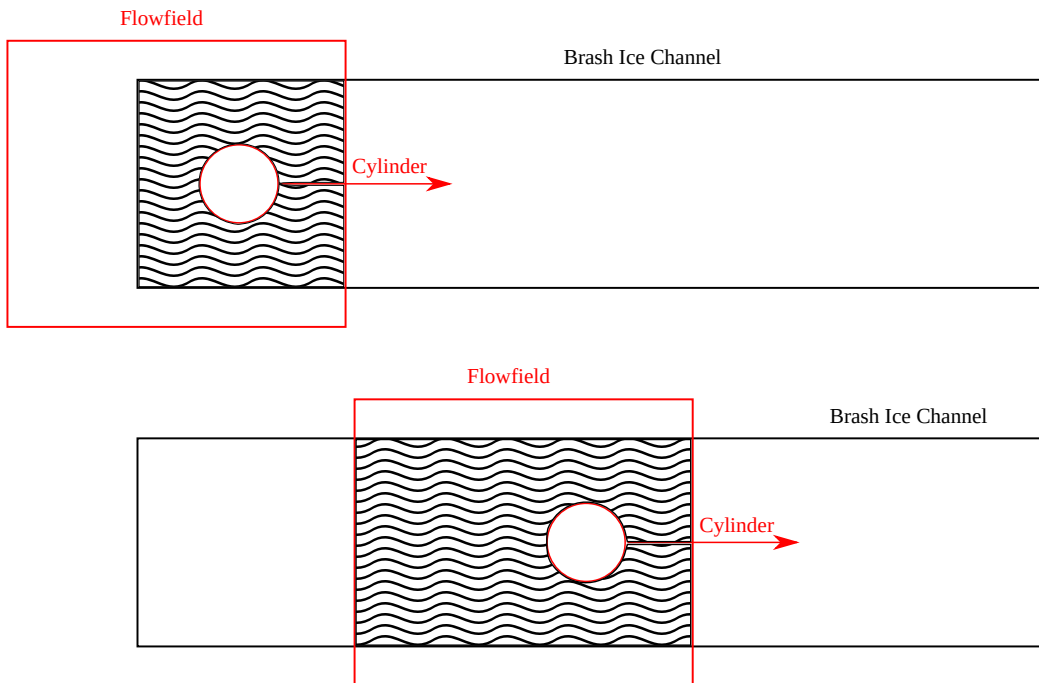


Figure 25: Flow field and brush ice channel domains [14]

Finally, brush ice particles detection when they are inside the flow field domain is carried out. Firstly, it is inspected that if the brush ice particle is inside the borders of imported

flow field. In case there is no brash ice particles detected inside the flow field region, the water velocity is calculated as zero. As for the brash ice particles inside the flow domain, the code calculates water velocity at the location of brash ice particle. This is accomplished by performing trilinear (x direction, y direction, and z direction, respectively) interpolation between the nodes, which surrounds the brash ice and carries the velocity-coordinates information of the flow field, and the brash ice location. This displayed in the color coded figure below.

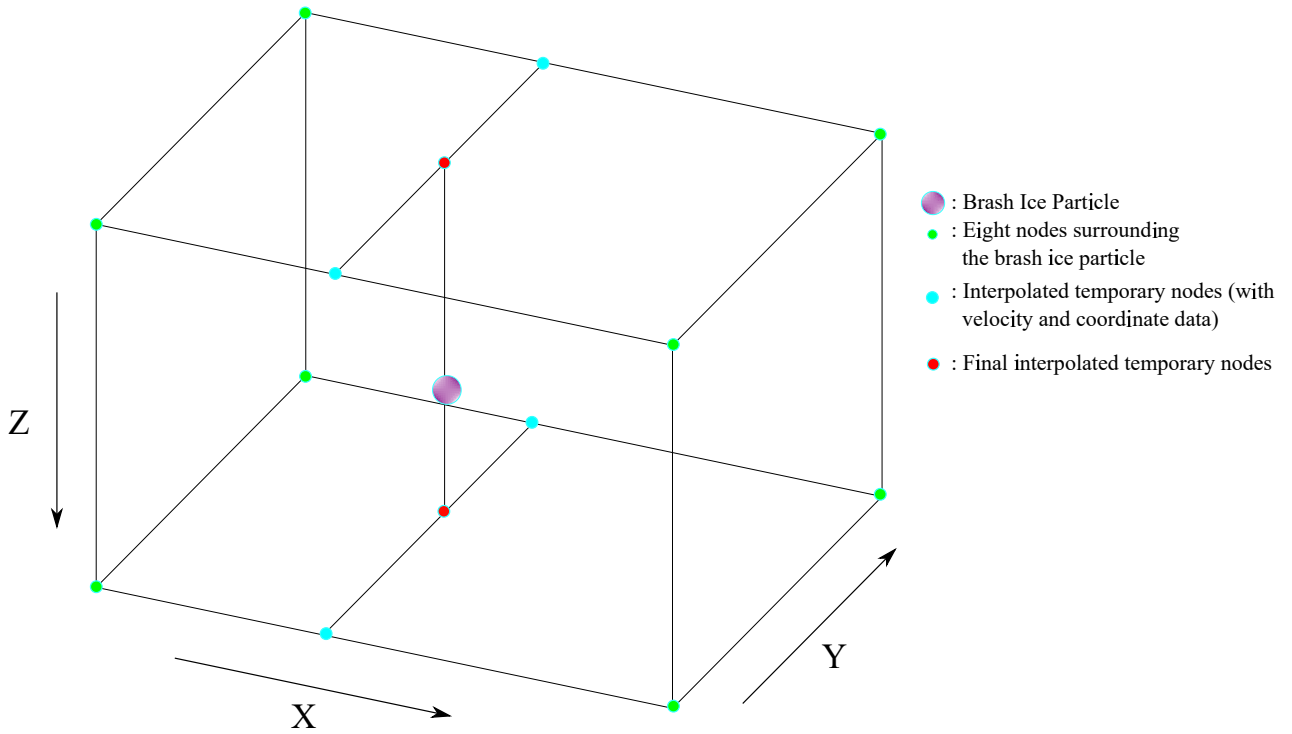


Figure 26: Trilinear interpolation [14]

### 3.4.3 Drag Force Computation

After calculation of the water velocity for the brash ice particles situated inside the flow field domain (figure-26), the drag force computation is realized.

Before any flow field was introduced into the code, the viscous drag computation of the ice particles was made based on brash ice particle's own velocity (due to the structure interaction) with still water assumption. It was calculated according to the following formula:

$$F_d = -C_w A \frac{1}{2} \rho (V_{BI})^2 \quad (7)$$

The same formula can be written in terms of relative water velocity observed from the brash ice particle. Drag force is acting on the same direction as the relative water velocity.

$$V_{BI} = -V_{w_{rel}} \longrightarrow F_d = -C_w A \frac{1}{2} \rho (V_{w_{rel}})^2 \quad (8)$$

where,  $F_d$ : drag force without hydrodynamic effect,  $C_w$ : drag coefficient of a sphere (taken as 0.47),  $A$ : cross section area of particles,  $\rho$ : water density,  $V_{BI}$ : velocity of brash ice particle,  $V_{w_{rel}}$ : relative water velocity observed from brash ice particle.

After introducing the flow field, the actual water velocity contributes to the total velocity of the particle. The resultant water velocity ( $V_{res}$ ) observed from the brash ice particle is obtained through superimposing the brash ice particle's relative water velocity ( $V_{w_{rel}}$ ) with actual water velocity ( $V_{w_f}$ ). This is illustrated in the figure below.

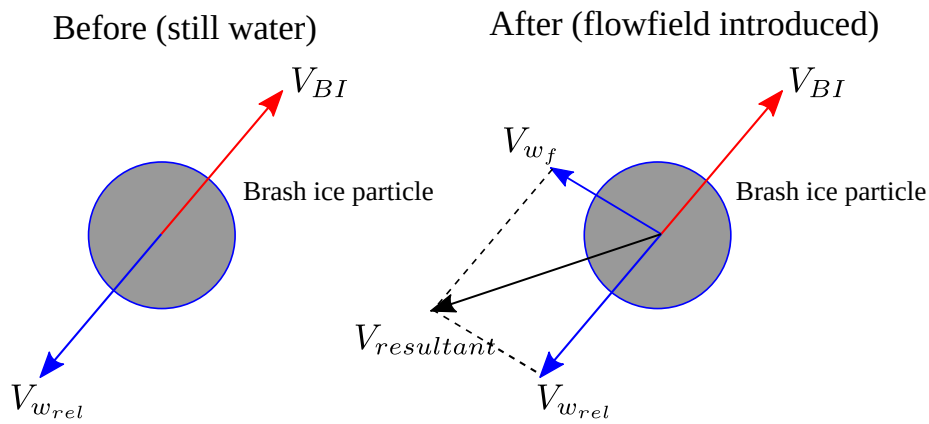


**Figure 27:** Brash ice velocity diagram before and after inserting a flow field [14]

After that, the resultant velocity ( $V_{rel}$ ) is plugged into the drag force calculation.

$$V_{resultant} = V_{w_f} - V_{BI} \longrightarrow F_{d_h} = -C_w A \frac{1}{2} \rho (V_{resultant})^2 \quad (9)$$

where,  $F_{d_h}$ : drag force with hydrodynamic effect,  $V_{w_f}$ : velocity of water

### 3.5 Area of Improvement

Improvements on the already existing hydrodynamics module of the code will be within the scope of this study. The existing tool only allows to import one flow field inside the DEM calculation (brash ice simulation), and only made available for cylinder experiment. Therefore, the main goal of this study is to improve the existing hydrodynamic capability

of the tool so that importing multiple flow fields into the tool will be possible. For this purpose; first, the CFD simulation for propeller will be carried out by modelling the propeller as an actuator disk. Volume force distribution over the actuator disk region will be defined to represent the momentum transferred to the fluid. After that, the code will be modified to insert multiple flow fields. The second aim of this work is to introduce the actuator disk simulation type into the DEM tool so that it can be directly executed from the DEM tool for given parameters by the user. The actuator disk simulation executed from the DEM tool should be able to save the results such as the actuator disk flow field and residuals automatically, without opening the GUI (graphical user interface) of ParaView. After that, the improved tool will be validated with the cylinder test using the actuator disk flow field and cylinder flow field acquired from the CFD department at the HSVA. Eventually, after validating the improved tool, the CFD simulation for the ship will be carried out. Then, the model ship simulation in brash ice will be executed with two flow fields imported to the code: the actuator disk and ship flow fields. Finally, the visual comparison between the simulation results and the experiment will be made.

## 4 Flow Field Around Propeller

The purpose of this simulation is to introduce a small tool to simulate the flow field of a propeller using a simple model. So as to reduce the computational cost, instead of using an actual propeller model, the propeller is modelled as an actuator disk in which the momentum transmitted from the propeller to the fluid is estimated and added to the fluid within the actuator disk region [17]. In the scope of this study, the forces exerted by the propeller on the brash ice particles are more significant than the details of the wake created by the propeller blades' rotation (swirl motion). Therefore, a steady-state, single phase actuator disk simulation is carried out to simulate the flow around propeller.

### 4.1 Actuator Disk Theory

In this approach, a uniform volume force over the actuator disk region is added to imitate the momentum transferred to the fluid. In order to implement this method, the propeller characteristics such as torque, thrust, and propeller diameter must be known in advance to compute the volume force. The volume forces computed such that it follows the Goldstein optimum distribution. As a result, the volume forces have a distribution in the following form [17]:

$$\mathbf{f}_{bx} = A_x r^* \sqrt{1 - r^*} \quad (10)$$

$$\mathbf{f}_{b\theta} = A_\theta \frac{r^* \sqrt{1 - r^*}}{r^*(1 - r'_h) + r'_h} \quad (11)$$

$$r^* = \frac{r' - r'_h}{1 - r'_h}, r' = \frac{r}{R_P}, r'_h = \frac{R_H}{R_P} \quad (12)$$

and the constants  $A_x$  and  $A_\theta$  are determined according to the fact that the volume force described over the actuator disk region is the summation of the total imposed thrust  $T$  and torque  $Q$ . Therefore,  $A_x$  and  $A_\theta$  are calculated as follows [17].

$$A_x = \frac{105}{8} \frac{T}{\pi \Delta (3R_H + 4R_P)(R_P - R_H)} \quad (13)$$

$$A_\theta = \frac{105}{8} \frac{Q}{\pi \Delta R_P (R_P - R_H)(3R_P + 4R_H)} \quad (14)$$

- $\mathbf{f}_{bx}$ : axial volume force

- $\mathbf{f}_{b\theta}$ : tangential volume force
- $R_P$ : exterior radius of actuator disk
- $R_H$ : interior radius of actuator disk
- $\Delta$ : thickness of actuator disk (projected into x-z plane or the length of the actuator disk)

The derivation of formulas for  $A_x$  and  $A_\theta$  can be found in Erik Svennings report [17]. The figures below display the normalized axial and tangential volume forces plotted against the normalized radius showing that the equations given above estimate a volume force distribution having a maximum value between  $r = R_H$  and  $r = R_P$ ; on the other hand, it decreases to zero at  $r = R_H$  and  $r = R_P$ .

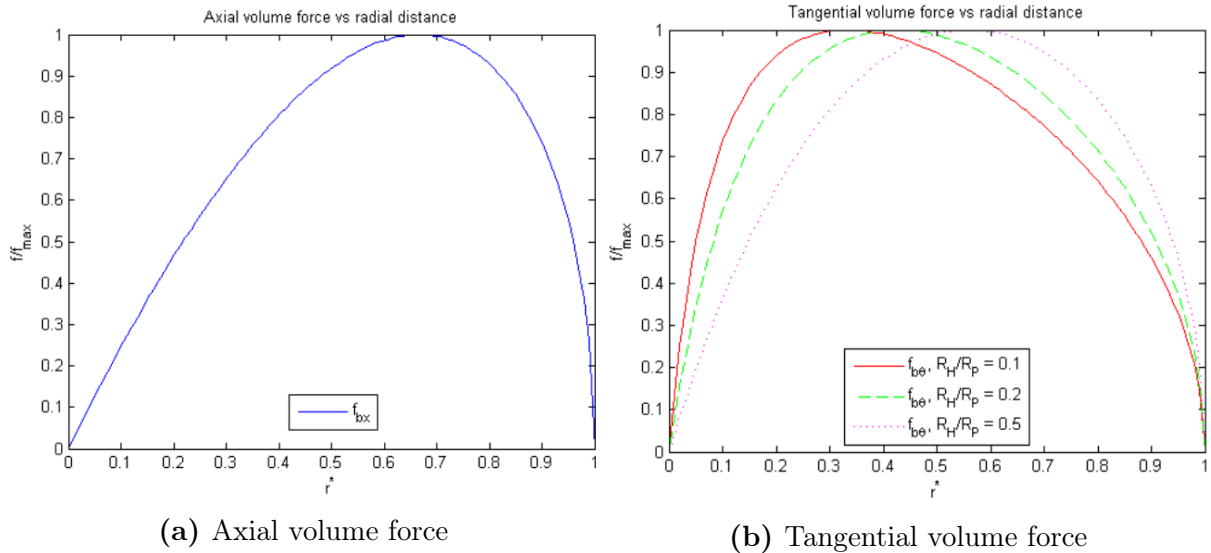


**Figure 28:** Normalized volume forces versus normalized radius [17]

After running the simulation with the volume force distribution applied, it is stated that distribution of pressure and tangential velocity over the actuator disk will be the same as the volume force distribution [18].

## 4.2 Properties of the Propeller

The HSVA model propeller used for the CFD simulation and its basic characteristics are given in the table below. For confidentiality reasons, the numbers are rounded.

Propeller Characteristics	
Scale ( $\lambda$ )	34
Propeller diameter $D_P$ [m]	0.25
Hub diameter $D_H$ [m]	0.5
Hub ratio $D_H/D_P$	0.2

**Table 2:** Basic characteristics of propeller

As mentioned earlier, the propeller is modelled as an actuator disk in the CFD simulation; therefore, the propeller thrust and torque must be given as inputs to the CFD simulation to calculate the volume force accordingly. Thrust at self propulsion point is selected for input which is approximately  $T = 44[N]$ . As for the torque, it is computed by using the propeller curve ( $K_T$ - $K_Q$ ) according to the given advance speed ( $Q = 1.1N.m$ ). The geometry of the actuator disk is given as an output in .vtk format when the simulation is executed.

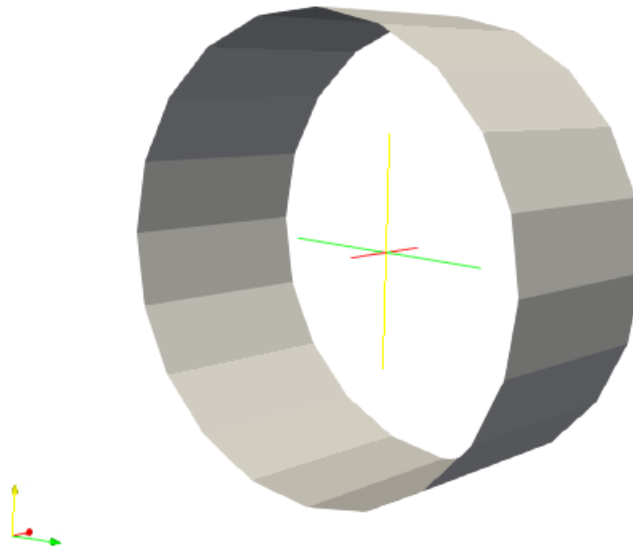


**Figure 29:** Actuator disk

### 4.3 Numerical Spatial Domain

The main difficulty when simulating the flow around propeller is that the mesh generation process becomes highly complicated due to the complex shape of propeller blades. Therefore, modelling the propeller as an actuator disk instead of using actual geometry is favorable to avoid complicated mesh near the propeller.



As for the spatial domain, the actuator disk is located at 4D distance from the inlet and 20D distance from the outlet. Also the radius of the domain is approximately 10D. The spatial domain with structural discretization is shown in the figures below together with the actuator disk (colored in dark blue in the figure-30a).

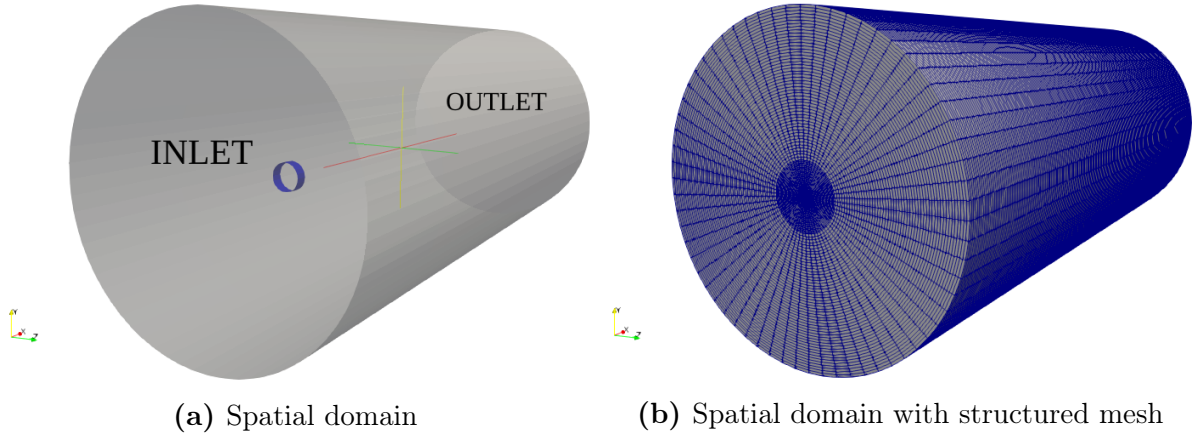


**Figure 30:** Spatial domain and its discretization

The mesh is generated by making use of openFoam’s `blockMesh` utility, and it involves 859520 hexahedral cells. The important parameters to assess the quality of the mesh is given in the table below.

	Average	Maximum	Threshold level
<b>Non-orthogonality</b>	2.65	36.75	65
<b>Skewness</b>	-	0.51	4
<b>Aspect ratio</b>	-	31.31	-

**Table 3:** Mesh quality of the actuator disk domain

#### 4.4 Simulation Setup

The simulation is carried out using a modified version of `simpleFoam` which is an OpenFOAM solver used for steady-state problems with incompressible, turbulent flows. This solver is modified in order to define the presence of an actuator disk and the volume force [17]. Furthermore, the solver employs SIMPLE algorithm to solve continuity and momentum equations which are given in the following.

$$\nabla \cdot \mathbf{u} = 0 \quad (15)$$

$$\nabla \cdot (\mathbf{u}\mathbf{u}) + \nabla \cdot (v\nabla\mathbf{u}) = -\nabla p \quad (16)$$

where,

- $\mathbf{u}$ : velocity field
- $\nabla p$ : relative pressure field divided by density ( $\rho$ ).
- $v$ : kinematic viscosity

Dirichlet (*fixedValue*) and Neumann (*zeroGradient* and *fixedGradient*) boundary conditions are defined at the inlet for velocity and pressure, respectively. In case of the Dirichlet boundary condition, the velocity value is explicitly defined. On the other hand, in the Neumann boundary condition, the velocity gradient is equal to zero in the direction perpendicular to the boundary. The velocity at the outlet is defined as *inletOutlet* which switches between the Neumann and Dirichlet boundary conditions. In case of the backward flow next to the boundary where the velocity vector points inside the domain, it switches to the Dirichlet boundary condition; if opposite, it switches to the Neumann boundary condition. The table below sums up the boundary conditions applied in the simulation.

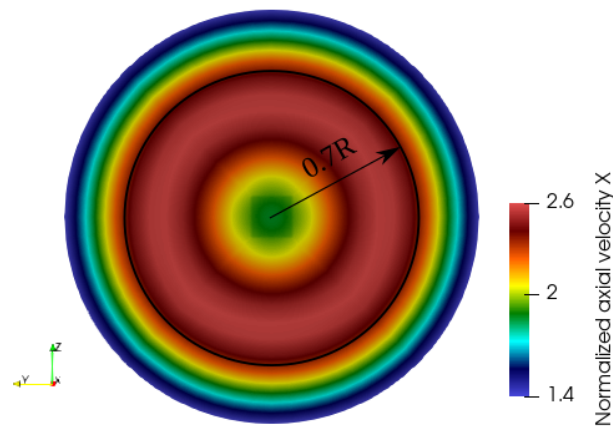
Boundary	Velocity boundary condition	Pressure boundary condition
Inlet	Dirichlet	Neumann
Outlet	<i>inletOutlet</i>	Dirichlet
Wall	<i>slip</i>	Neumann

**Table 4:** Boundary conditions for actuator disk simulation

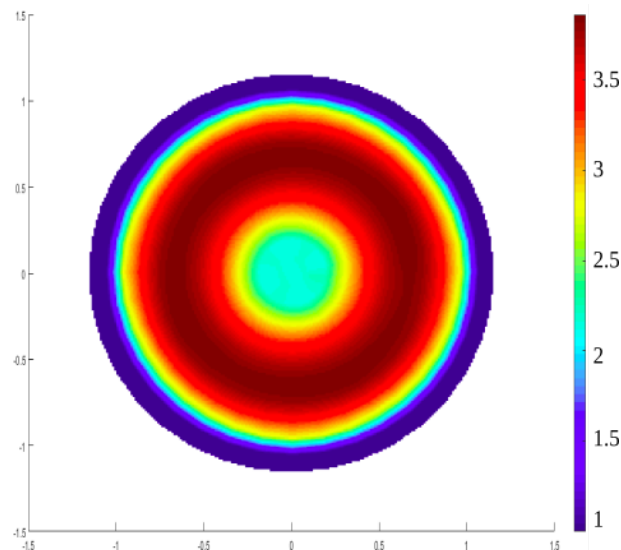
The velocity defined at the inlet and the internal field is  $0.352m/s$  in the x direction. Moreover, the kinematic viscosity and the density of the fluid are defined as  $v = 1.56e - 06m^2/s, \rho = 1005.5kg/m^3$ , respectively. Furthermore, *SSTk -  $\omega$*  turbulence model is selected and prescribed at the boundaries of the fluid domain. The selection of turbulence model is based on the master thesis written by Borna Šeb [18] who performed a simulation for propeller model using actuator disk theory. Finally, the numerical schemes used to discretize the divergence term ( $\nabla \cdot$ ) of the momentum equation are selected as linear upwind scheme.

## 4.5 CFD Simulation Results

Simulation results are presented in this section. The results are represented in terms of axial velocity distribution normalized by inflow (inlet) velocity ( $U/0.352$ ) over the actuator disk and the numerical domain. Another simulation was performed by the CFD department with the similar propeller characteristics at the HSVA in order to confirm the axial velocity distribution obtained through OpenFoam. The figures below compare the normalized axial velocity obtained through OpenFoam and the results obtained through the HSVA propeller panel code provided by the CFD department. This comparison is made in order to confirm the axial velocity distribution. The images are taken from one radius behind the propeller.



(a) Normalized axial velocity



(b) Normalized axial velocity by HSVA propeller panel code

**Figure 31:** Comparison of normalized axial velocities

As it can be inferred from the figure-31a, the maximum axial velocity is almost achieved at 70% radius of the actuator disk (shown in black circle) as well as for the simulation performed via the propeller panel code by HSVA. Therefore, it can be deduced that the axial velocity distribution is quite similar to the simulation done by the HSVA, validating the results from OpenFoam.

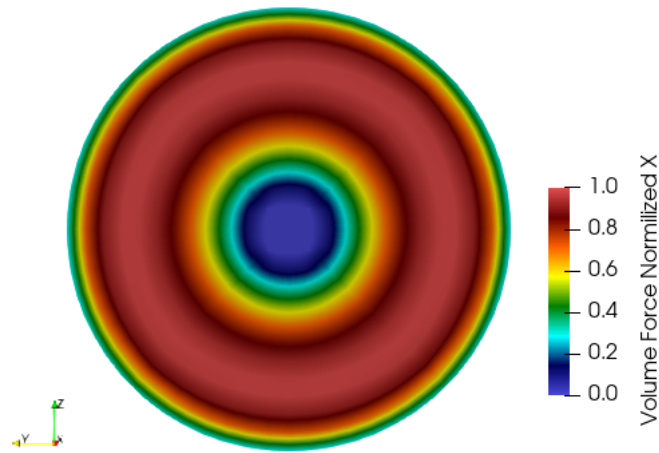


**Figure 32:** Normalized axial volume force

Furthermore, it can be deduced that the the velocity distribution is similar to the volume force distribution shown in 32. As it was stated before in the section-4.1, the axial velocity jump tends to decrease at the hub region of the propeller; and it increases gradually by following the prescribed distribution mentioned earlier, as the normalized radius increases (see figure-28). Furthermore, the side view of the velocity distribution along the numerical domain will be presented in the following sections in order to make a comparison with the results obtained through the flow field conversion simulation.

The convergence history of the residuals is also presented in the following figure to assess the validity of the results.

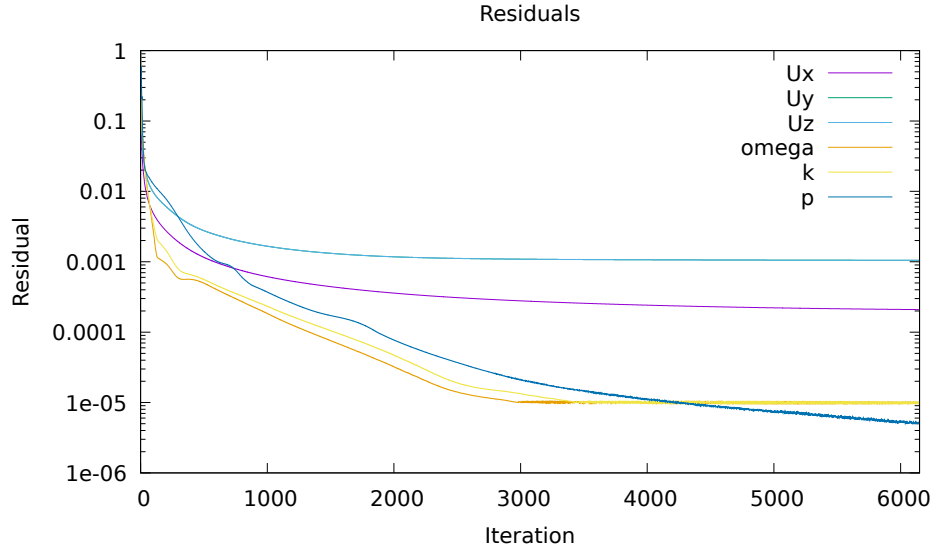


**Figure 33:** Convergence history for actuator disk simulation

Although all the residuals should be at least below  $10^{-4}$  to have a converged solution, the results are found to be good enough to proceed with further analysis made for brash ice simulations; since the qualitative assessment of an ice particle behaviour under the influence of multiple flow fields is the main aim of this work.

#### 4.6 Automating the Actuator Disk Simulation

The actuator disk simulation case is plugged into the DEM code as a new simulation type so that the user can also perform an actuator disk simulation to obtain a flow field around a propeller. To do so, the main shell script named `RunActDiskCase` is created to be called inside the DEM code to execute the CFD simulation. A basic user interface is created, asking the user for basic parameters of the simulation before running the simulation such as inflow velocity, density, and position, thrust, torque, radius of an actuator disk. Parallel run is also optional. Furthermore, after the simulation is started, it creates and checks the quality of the mesh, and saves them into a `log` file to be checked by the user. Moreover, if the simulation is interrupted by the user, the user can execute the same simulation again from the latest time step and attaching the shell output into the already existing (created when the simulation run for the first time) `log` file. That way there will not be any missing information in the `log` file that saves the residual information of the parameters at every iteration to be plotted afterwards.

Furthermore, in order to acquire the flow fields as a `.txt` file after the simulation ends, a

python script is written which exports the velocity-point coordinate data automatically from Paraview (open-source scientific visualization tool) without opening its GUI (Graphical User Interface). The python code processes the raw data visualized in Paraview in order to make the data compatible with the DEM tool. Also, another shell script is created (`ResPlot`) to plot the residuals and save as `.png` after the simulation. These scripts are called inside the main shell script mentioned earlier. A figure is given below, showing the interface created for the user when executing the actuator disk simulation from the DEM code.

```
!=====  
!      Actuator Disk Openfoam 2.4.0 Simulation      !  
!=====  
  
-> Working directory for openfoam : Default/ActDiskSim  
Sourcing the OpenFOAM 2.4.0 environment...  
RUNNING FOR THE FIRST TIME  
+++++  
+++++Input Propeller Data+++++  
+++++  
Do you want to enter the propeller input (x,y,z,rho,T,Q,r,U)? [y,n]y  
Start point of the actuator disk x coordinate=0.95  
Start point of the actuator disk y coordinate=0  
Start point of the actuator disk z coordinate=0  
Three coordinates has been taken (x,y,z).  
End point of the actuator disk x coordinate=1.05  
End point of the actuator disk y coordinate=0  
End point of the actuator disk z coordinate=0  
Three coordinates has been taken (x,y,z).  
x component of the initial velocity field=0.352  
y component of the initial velocity field=0  
z component of the initial velocity field=0  
Three components has been taken (x,y,z).  
Enter the thrust [N] =43.6207  
Enter the torque [N.m] =1.101  
Enter the density [kg/m^3] =1005.5  
Enter the hub diameter [m] =0.019  
Enter the propeller diameter [m] =0.11745  
blockMesh has been created.  
Mesh has been checked.  
Do you want to run in parallel? [y,n]
```

Figure 34: Actuator disk CFD simulation interface

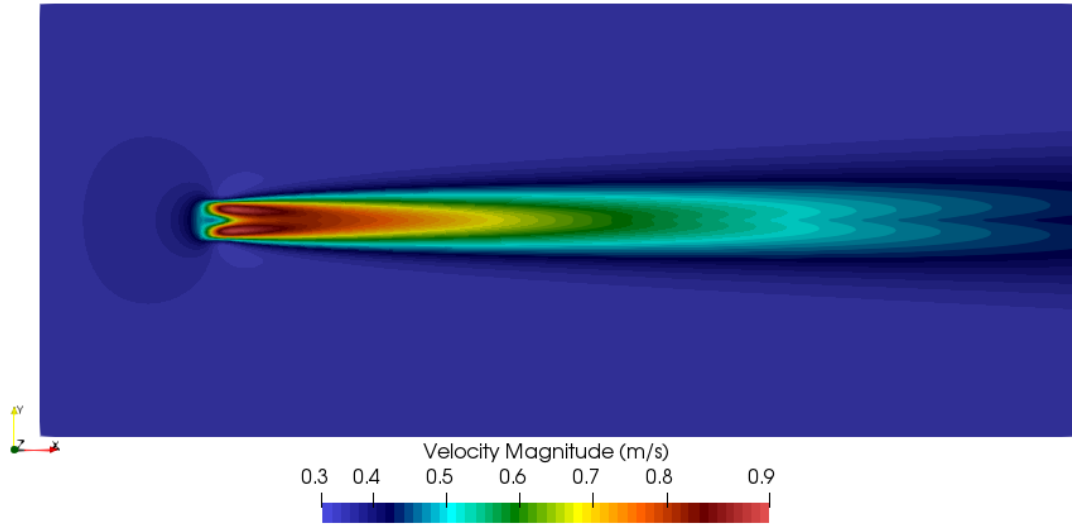
Finally, another shell script is written to reset the simulation case `CleanActDiskCase` which is added to the DEM code as an option. As a result, the actuator disk simulation case is automated to execute the actuator disk CFD simulation for different types of propellers without requiring any knowledge regarding the OpenFoam file directory.

## 4.7 Flow Field Conversion

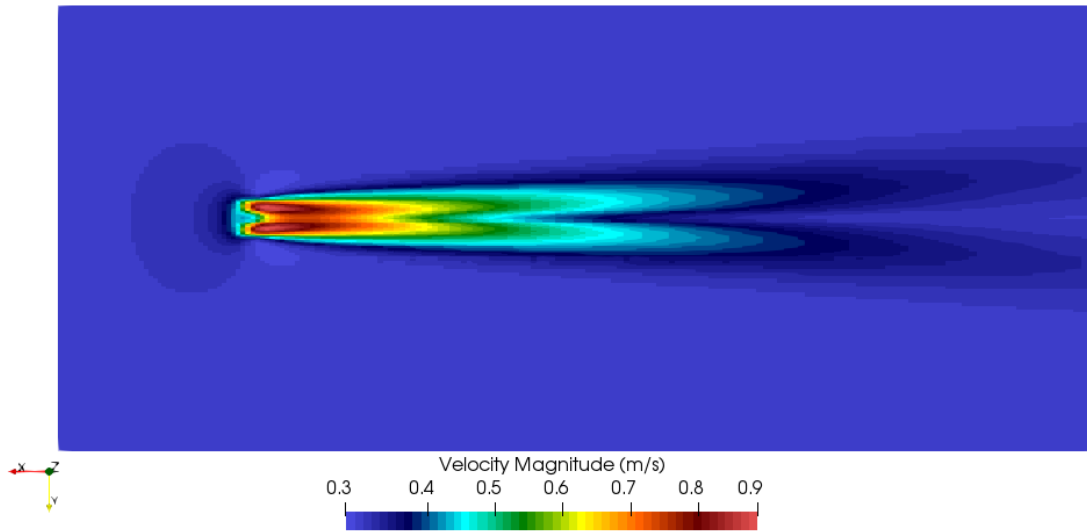
As explained earlier, to import the CFD flow field into the brash ice simulation, the CFD grid must be simplified. The flow field conversion simulation has two parameters to be taken into account when it comes to making a compromise between the computation time

and the quality of the results: the minimal distance between nodes in the newly generated structured grid ( $d_{gn}$ ) and the tolerance in the matching process ( $tol$ , see the green circle in the figure-23) [14].  $d_{gn}$  defines the number of nodes created in the converted grid. The smaller  $d_{gn}$  is, the more number of points are created in the new grid. The tolerance value ( $tol$ ) is defined after the generation of the new grid to adjust the number matched nodes. When the tolerance value ( $tol$ ) increases, the amount of matched nodes between the CFD grid and the new grid also increases.

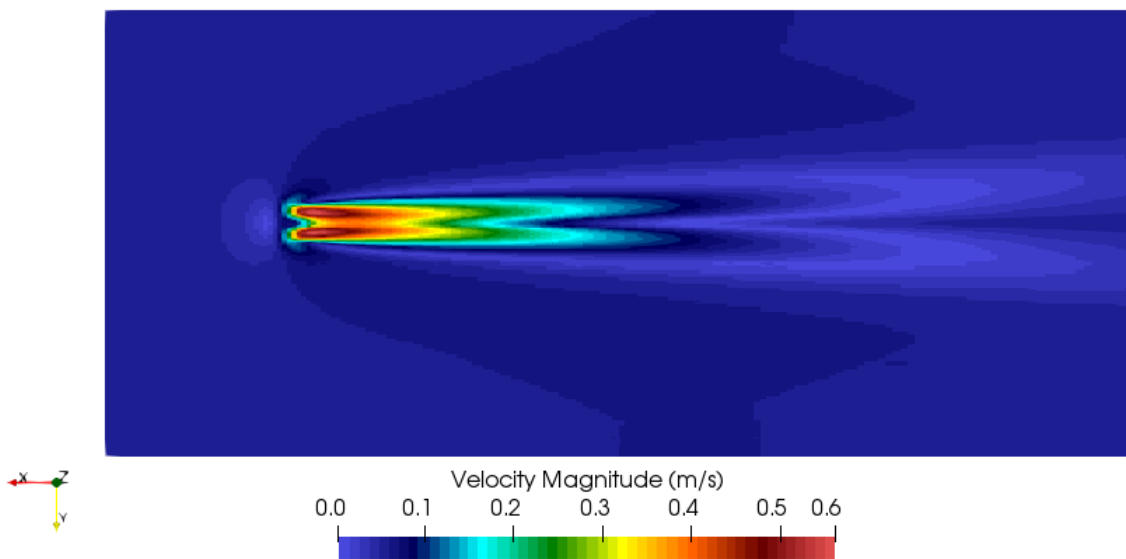
The parameter study was conducted by Sophie Demmin [14] to observe the effect of these parameters on the quality of the results as well as the computation time. As a result, it was found that the computing time depends on  $d_{gn}$  to a great extent; and the tolerance value has almost no effect on the computing time [14]. However, for the greater values of tolerance, the quality of the new grid, which depends on the number of matched nodes (found nodes) that involves the CFD velocity data, increases. Therefore, it is concluded that  $tol$  value should be kept as large as possible to acquire a good quality grid. On the other hand,  $d_{gn}$  number also should be large enough to have enough number of points in the newly generated grid. In conclusion,  $d_{gn}$  and  $tol$  values are set to be  $5mm$ , and  $20mm$ , respectively, for the actuator disk flow field conversion. The result of the converted flow field for the actuator disk flow field is given in the figure below in comparison with the actual CFD velocity field.



(a) Velocity field for CFD simulation



(b) Velocity field for converted flow field



(c) Velocity field for converted flow field after subtraction of internal velocity defined in CFD

**Figure 35:** Comparison of actuator disk velocity fields between converted flow field and CFD flow field



The figure-35b represents the converted flow field without subtracting the inflow velocity field defined in CFD simulation. Therefore, it is an ideal view to compare with figure-35a in order to see the difference between CFD flow field and interpolated flow field. The figure-35c represents the final converted flow field to be used in DEM simulations.

In the CFD simulation, the initial velocity was defined at the inlet and the internal domain as mentioned earlier. In other words, the actuator disk was stationary and the constant velocity of the flow was defined in the entire CFD domain. However, in the brash ice simulation, the actuator disk moves with the structure (cylinder or ship) through the channel and the flow field remains stationary. Therefore, when converting the CFD flow field, the initial velocity defined in the CFD domain must be subtracted from the velocity field to be used in the brash ice simulation reference frame. It can be seen from the figure-35c that the internal velocity field is almost zero everywhere except for the propeller downstream (-x direction in figure-35c) where only the actuator disk volume force accelerates the flow field. It is also worth mentioning that the x-axis orientation of the original flow field is changed to the opposite for the converted flow field, as seen in the comparison above, in order to adopt the flow field to the axis orientation of the brash ice simulation.

## **5 Further Improvements on Hydrodynamic Module**

In this section, the improved tool will be described. The validation study will be carried out by utilizing the velocity fields for the cylinder and actuator disk. After the proof of the modified tool, the brash ice ship model simulation will be solved with the modified tool and the results will be discussed.

### **5.1 Description of Improved Tool**

The modifications are performed mainly on the hydrodynamic module of the tool. As explained in detail before, this module involves subroutines for importing the flow field, detecting brash ice particles drops inside the flow field domain, and calculating the velocity at the location of brash ice particle by making use of the trilinear interpolation.

The first adaptation is made on the subroutine that imports the flow field. After generating the CFD results with simplified mesh by using the grid conversion simulation, the

created flow fields are output in separate folders named in order (eg. Flowfield1, Flowfield2 etc.). After that, when the simulation for the cylinder or ship is executed, the loop over all flow fields is done in order to pass the information from all flow fields that are in `.txt` files into arrays. Every flow field is described as derived data types consisting of data objects of different types such as coordinate and velocity arrays. A modified version of the figure-24 is given in the following figure to understand the flow field data structure better.

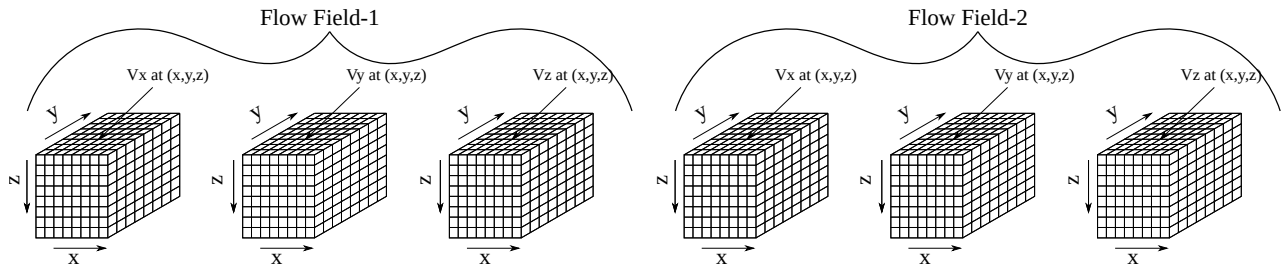


**Figure 36:** 3-D velocity arrays for multiple flow fields

The second modification is performed on the relocation of the flow field when the brash ice simulations are executed. The original tool was adjusted according to the cylinder flow field in which the flow field already meets with the cylinder origin, meaning that the origin of the CFD and the brash ice simulation coincides. However, the CFD simulation does not necessarily has to coincide with the origin of the brash ice simulations. As it will be introduced in the following sections, the model geometry in CFD simulations are placed with an offset from the fluid domain's origin (usually taken at the inlet). Therefore, simply coupling the flow field with the structure (cylinder or ship) by adding the structure's location to the flow fields' coordinate arrays in the DEM simulation is not sufficient. As a result, a `.txt` file is created for the code to read so as to offset every flow field in the brash ice simulations according to the distance of the CFD models from the origin of the CFD simulations. A color coded illustration is provided below similar to figure-26 but with multiple flow field's region. The configuration below will be later used in the proof of the modified tool and it represents an unrealistic set-up, a cylinder structure with one propeller each side.

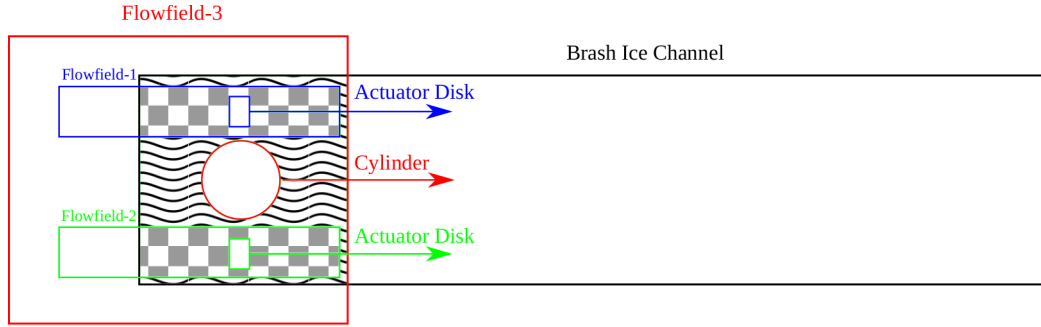


**Figure 37:** Domains of multiple flow fields and brash ice

After relocating the flow fields at every time step based on the CFD simulations, the last step is to determine the water velocity for the brash ice particles situated inside the flow field domains. Since there are many flow fields overlapping with one another (checkerboard region in the figure-37), the summation of the water velocities from every flow field is taken into account for the brash ice located inside the overlapped domain. The resulting water velocity observed from a brash ice particle is calculated the same way as described in section-3.4.3 (figure-27) with the only exception being that the actual water velocity acting on the brash particle has components coming from several flow fields. A modified version of figure-27 is given for multiple flow fields case imported into the tool.

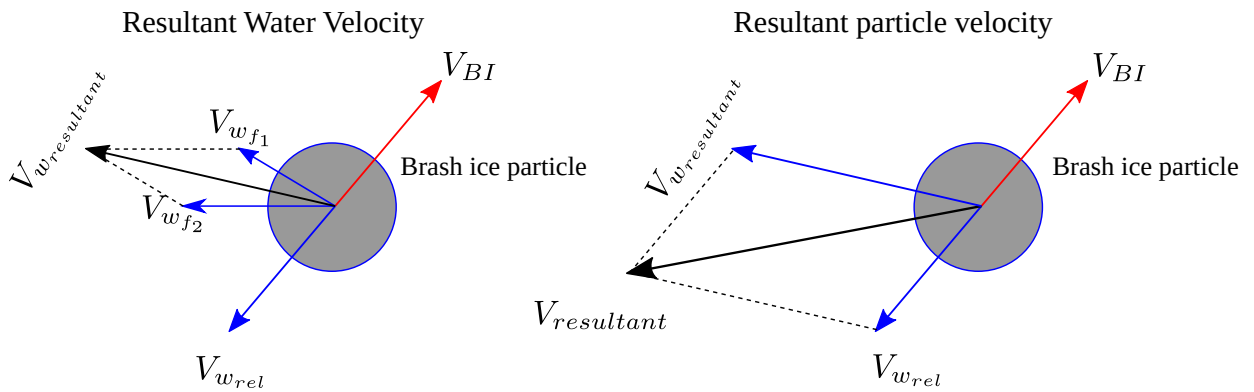


**Figure 38:** Brash ice velocity diagram for multiple flow fields

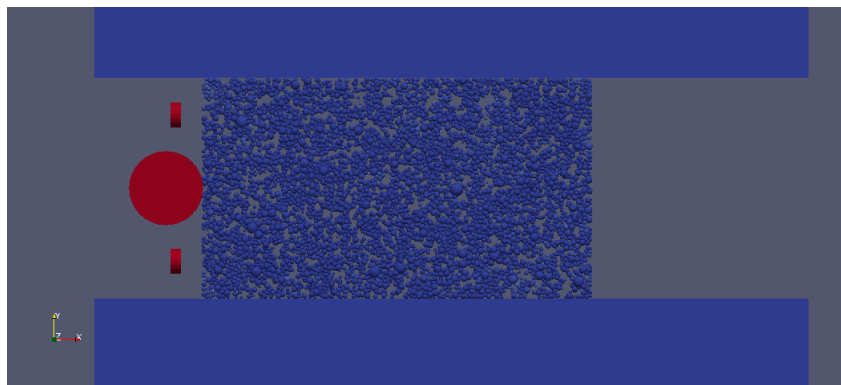
## 5.2 The Proof of Modified Tool

In this part of the study, the modified tool will be tested by inserting multiple flow fields: actuator disk flow field and cylinder flow field. The configuration mentioned in figure-37 will be used for checking the functionality of the modified tool. The flow field for the actuator disk was already acquired and simplified as explained in the previous chapter. As for the cylinder flow field, a CFD simulation was already performed by colleagues at

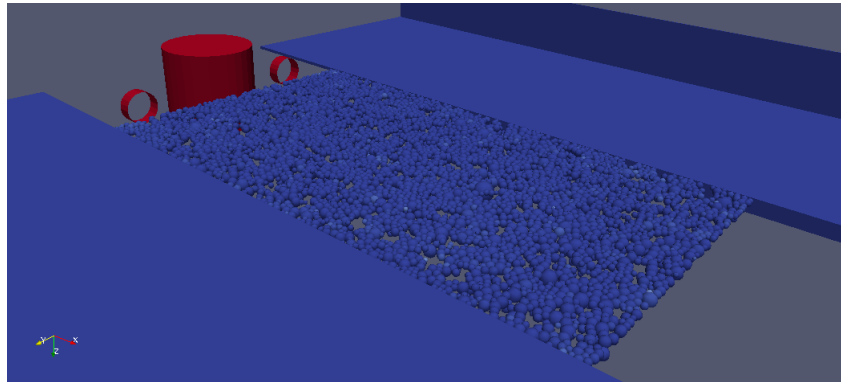
the CFD department of the HSVA as mentioned in Sophie Demmin thesis [14].

### 5.2.1 Cylinder Simulation with Improved Tool

In this section, the proof of the improved tool will be carried out. Three flow fields will be inserted into the brash ice simulation; one belongs to the cylinder, and the other two belong to the actuator disk. The converted flow field of actuator disk in figure-35c is duplicated and inserted into the DEM domain. The general view of the brash ice channel with the cylinder and the actuator disk positioned at the sides of the cylinder is given in the following figure.



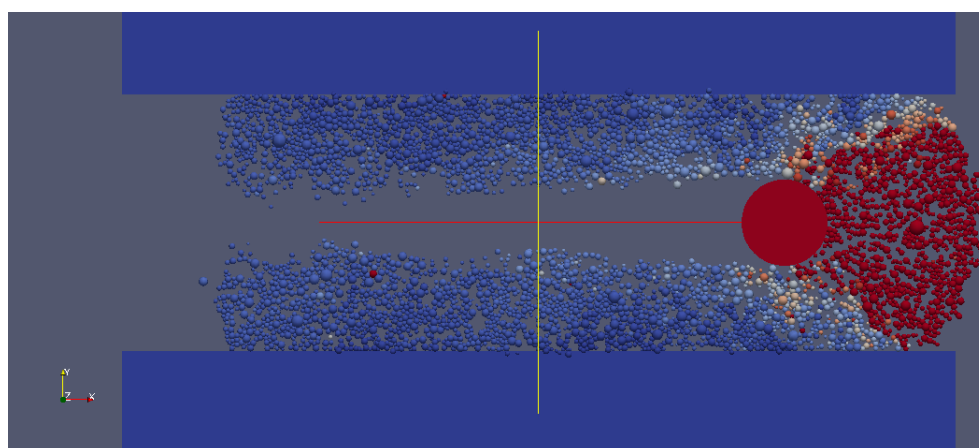
(a) Bottom view



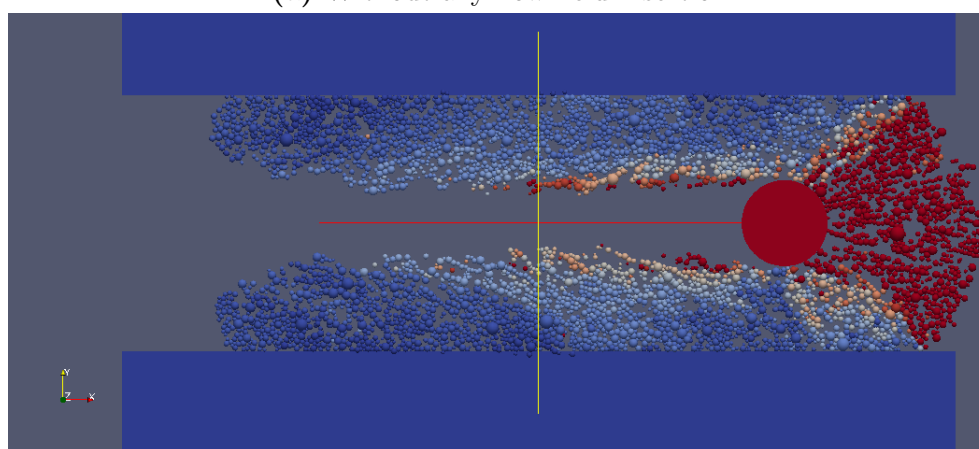
(b) Isometric view

**Figure 39:** The configuration of the cylinder brash ice simulation for validation study

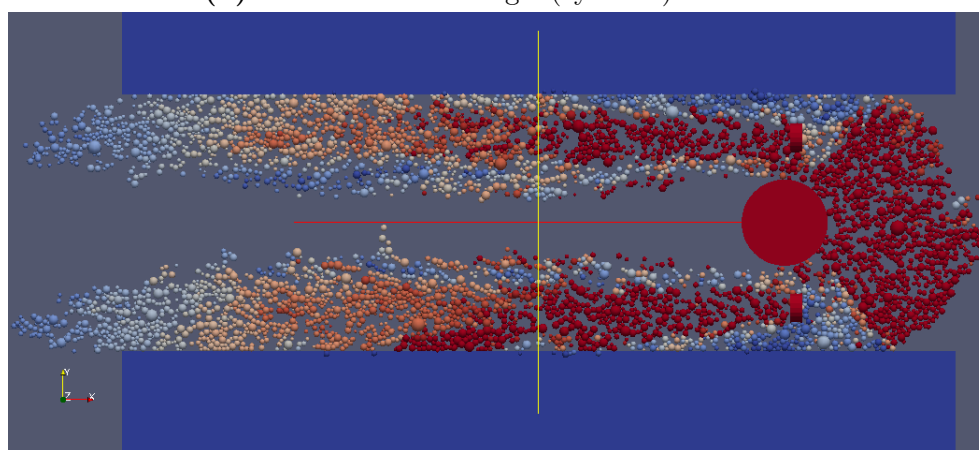
The flow fields are inserted into the cylinder simulation so as to verify the ability of the modified tool allowing to import multiple flow fields and affecting the brash ice particles' movement. The cylinder simulations are performed only to display the functionality of the modified tool; it is not a realistic set-up at all. The comparative results are given in the following figures.



(a) Without any flow field insertion



(b) Initial tool with single (cylinder) flow field



(c) Multiple flow field with improved tool

**Figure 40:** Comparison of cylinder brash ice simulations

In the figures above, the comparison is made between the improved tool with multiple flow field insertion (figure-40c), the simulation performed using the initial tool (figure-40b), and the cylinder simulation without any hydrodynamic effect considered in the particle movement as well as in the drag force computation (figure-40a). The effect of the actuator disk flow fields on the ice particle movement can be clearly observed in figure-40c when

compared to the figure-40b such that the particles are getting sucked into the actuator disk region and pushed back through the ice channel.

In order to visualize the actuator disk moving with the cylinder, there are two subroutines introduced into the tool. One of them reads the `.vtk` file that was output by the actuator disk simulation to visualize the actuator disk geometry in the simulation. The other one updates the actuator disk position in time by exporting `.vtk` files for each propeller and each graphic output step. Furthermore, the input file is created in order to take the propeller positions from the user.

In conclusion, it can be inferred that the improved tool is proved to be working well. Further analysis with the ship model simulation can be carried out.

### **5.3 Simulation of Model Ship Experiment**

In this section, the improved tool will be tested against the ship model simulation in brash ice. First, a CFD simulation will be carried out so as to determine the flow around the ship; after that, the acquired flow field will be simplified by the flow field conversion simulation; finally, the brash ice simulation will be executed with the actuator disk flow field and the ship flow field imported into the simulation.

#### **5.3.1 Flow Field Around Ship**

In this section flow field around the ship will be solved using OpenFoam. First the ship particulars and the 3-D model of the ship will be presented, then the simulation setup and the spatial domain will be described; after that, the CFD results will be presented.

##### **5.3.1.1 Ship Geometry**

The basic particulars of the model ship used in the CFD and DEM calculations are presented in the table below. The numbers are rounded due to confidentiality reasons. In the simulations, the exact values are used.

	Ship Data	Model Data
Model Scale	34	1
LOA [m]	7.5	250
Breadth [m]	1.3	43
Fwd. Draft Ballast [m]	0.2	6.5
Aft. Draft Ballast [m]	0.3	9.5
Disp. Ballast [ $m^3$ ]	1.6	62000
Speed [m/s]	0.44	2.58

**Table 5:** Main particulars of the model ship

The initial CAD model received involved many naked edges and manifold boundaries, making the model not suitable for CFD simulations. Therefore, the ship model is recreated with few simple surfaces by using the reference lines of the original CAD model. The skeg of the ship model is removed for simplification purposes. The original and the modified CAD geometry of the ship are given in the following figures.

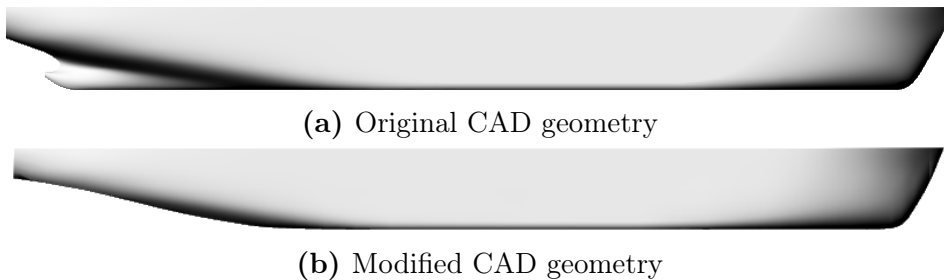


**Figure 41:** Original and modified ship geometry

### 5.3.1.2 Simulation Setup

The numerical domain used in the calculation is provided in the following figures along with the boundary definition. The inlet boundary is located approximately  $1.5L$  away from the inlet, and the outlet boundary is placed  $3.5L$  downstream.

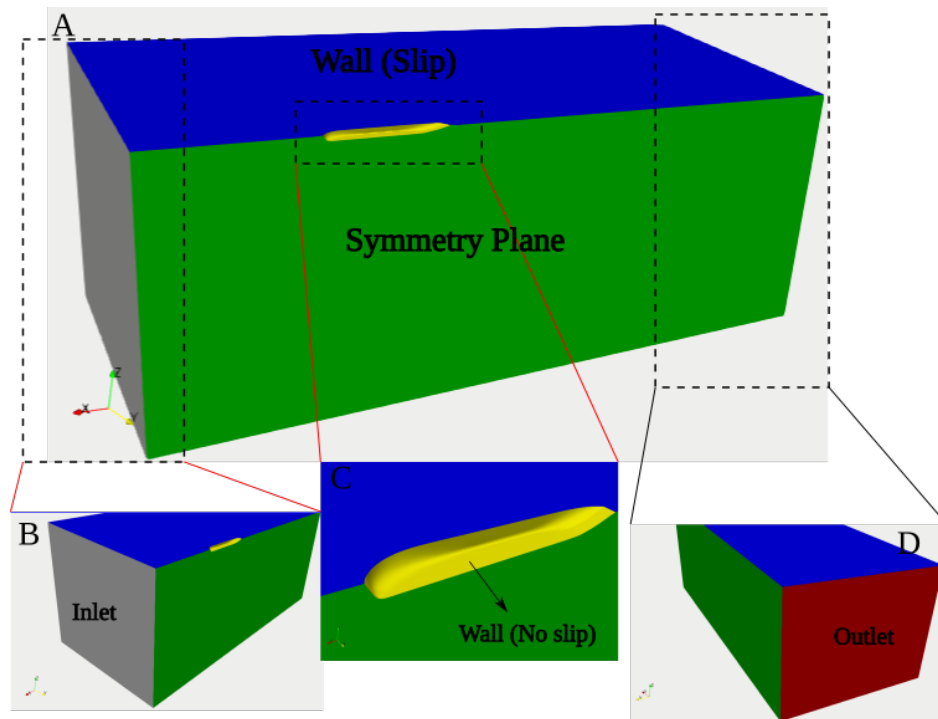


**Figure 42:** Numerical domain for ship simulation. A. general view of the numerical domain; B. zoomed view near inlet boundary; C. zoomed view near the hull model; D. zoomed view near outlet boundary

The mesh generation process for the ship CFD domain is performed in two phase in OpenFoam; first, the `blockMesh` utility is used in order to create hexahedral mesh for the domain, then the `snappyHexMesh` utility is used to generate a mesh around the ship which is defined as `.stl` file in the OpenFoam case file. Furthermore, the gradual decrease of the mesh size is controlled by the `topoSet` utility. As a result, 633050 hexahedral, 1180 prism cells are generated. The average  $y+$  value is kept around 26 along the hull. The spatial discretization of the numerical domain is displayed in detail in the following figure.



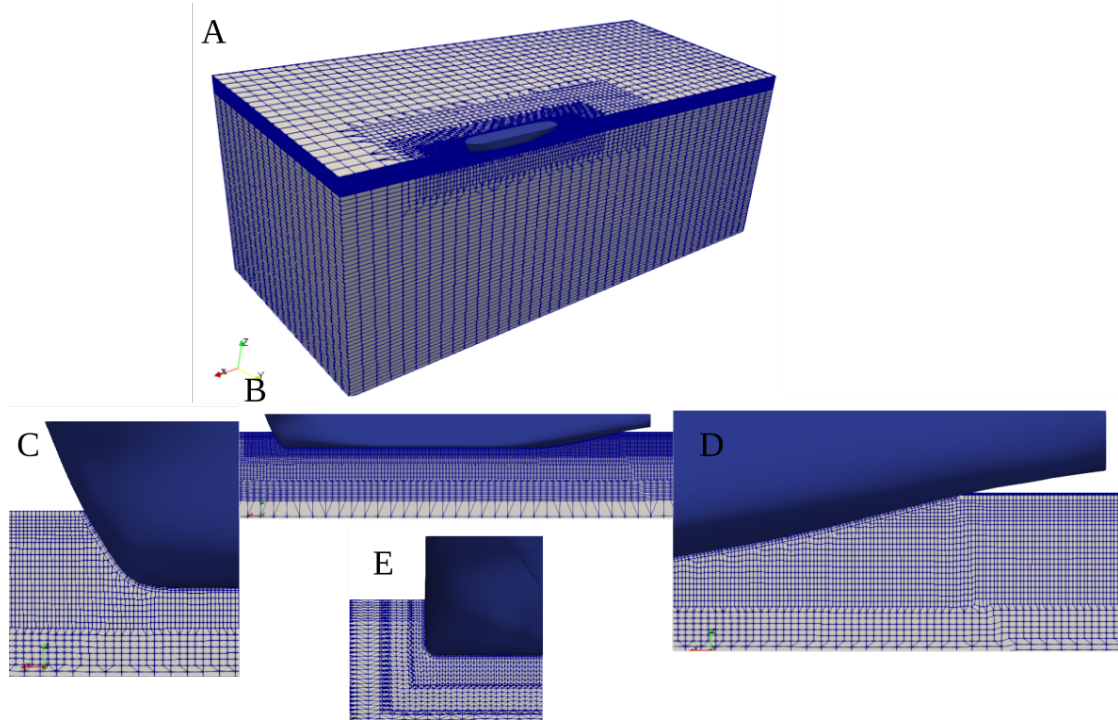


**Figure 43:** Discretized numerical domain for ship simulation. A. overall mesh; B. mesh around the ship; C. mesh around the bow; D. mesh around the stern; E. mesh around ship midsection

The flow field around the ship is also solved using OpenFoam's solver for steady-state, single phase, incompressible and turbulent flow (`simpleFoam`). Since the governing equations for this solver was introduced in the actuator disk CFD simulation (equation-16 and equation-15), it will not be repeated again here. The Reynolds Averaged Navier Stokes Equations (RANSE) are solved using the Shear Stress Transport (SST)  $k-\omega$  turbulence model. On the contrary to most of the applications found in literature (see section-2.4.3), the simulation is performed steady-state and single phase (water) for the ship due to the limited computation power of the personal computer of the author. However, since the effect of aerodynamic drag on brash ice particles is considerably lower than the hydrodynamic drag due to the density difference between water and air, a multi-phase flow field would not make much difference on the movement of the ice particles. And also, it is not expected to see any time dependent effect of the ship in the flow domain such as wave creation at specified advance speed ( $5knots$ ). Therefore, the computational domain is generated until the draught of the ship, without taking into account the free surface effect. The inflow velocity is defined at the inlet in the x direction as  $-0.44m/s$ .

### 5.3.1.3 CFD Simulation Results

In this section, the results of the flow around the ship are given in terms of convergence history (force and residuals). The distribution of velocity along the spatial domain will be given in the following section in order to make a comparison between the CFD flow field and the converted flow field for the brash ice model simulation.

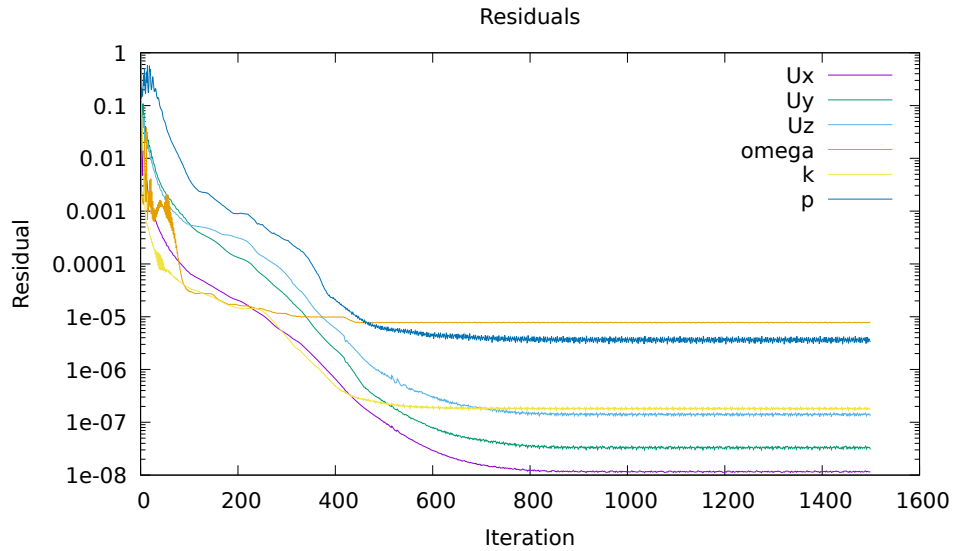


**Figure 44:** Residual convergence history for flow around the ship

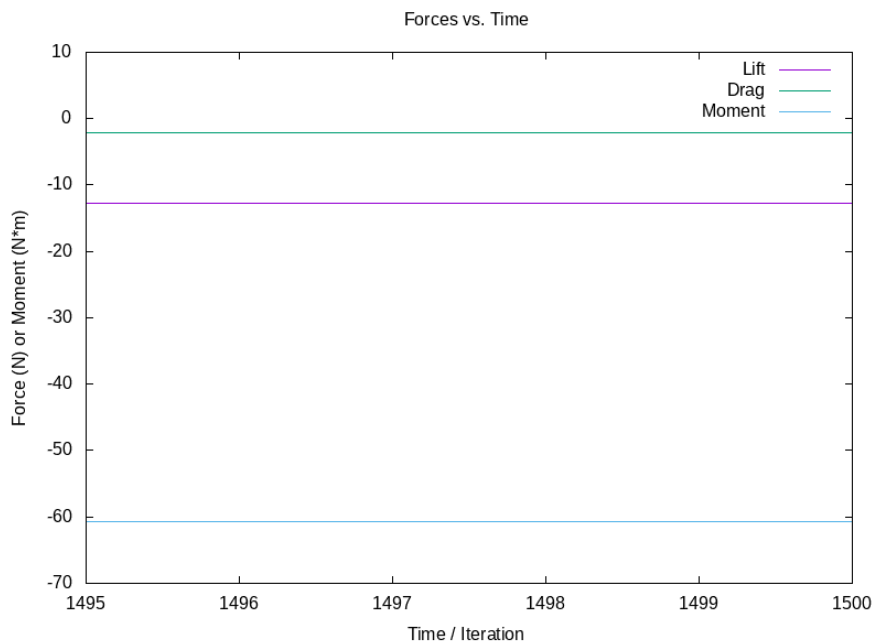


**Figure 45:** Force convergence history for flow around the ship (zoomed view)

It can be seen from the residual history graph in figure-44, all the residuals are below  $10^{-4}$ ; considered to be well converged. Furthermore, it can also be seen from the zoomed force

graph in figure-45 (showing only the 5 last iteration to check if there are any fluctuations) that the forces acting on the hull also converge. Although the DEM simulation does not require a high accuracy in the CFD flow field, these graphs show that the CFD results for the ship are good enough to proceed with further simulations regarding the flow field conversion and brash ice simulation.

### **5.3.2 Brash Ice Model Simulation**

After acquiring the flow around the ship, the brash ice simulation can be run by inserting the ship and actuator disk flow fields at the same time. First, the flow field conversion simulation (created by Sophie Demmin[14]) will be carried out and the converted flow field will be compared with the actual CFD flow field. After that, since the reference system of the CFD domain for the ship is different than the DEM tool, how to position the converted flow field in the brash ice model simulation will be explained. Finally, the brash ice model simulation will be executed with the improved tool allowing for multi-flow field insertion into the brash ice simulations.

#### **5.3.2.1 Flow Field Conversion**

In order to reduce the computational burden, the flow domain of interest around the ship is extracted for the flow field conversion simulation. The domain of interest is shown in red in the figure below. It is reflected from the symmetry plane.

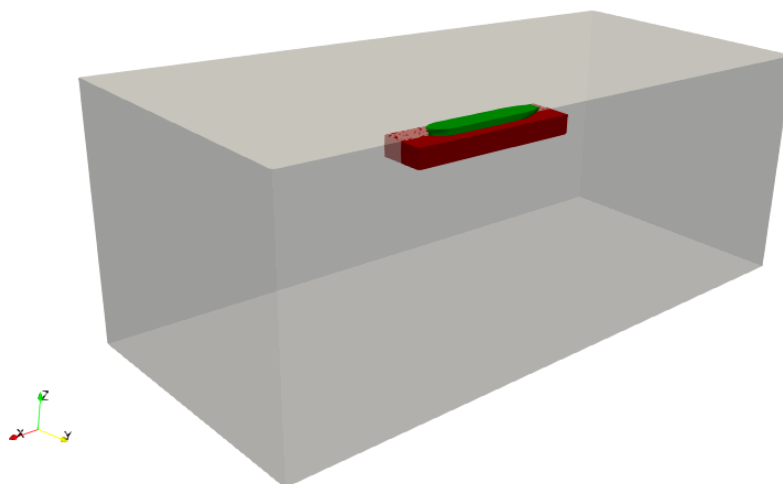


**Figure 46:** Extracted domain for the flow field conversion simulation (red: extracted domain, green: hull, grey: entire numerical domain)

Furthermore, just like the actuator disk simulation, the velocity distribution comparison is

made between the converted flow field and CFD flow field. The bottom and side velocity distributions for both cases are presented in the following figures.

It can be seen from the following figures that the axis orientation of the converted flow field, which is used in DEM simulations, is different than the CFD axis orientation. The z-axis orientation is in opposite direction for the DEM simulation compared to the CFD simulation. Therefore, these axis orientations must be managed manually in the flow field conversion simulation depending on the configuration of the CFD simulations. Another significant remark is that the inflow velocity defined in the CFD simulation where the ship is stationary and the water is moving must be subtracted from the CFD flow field in order to adjust the flow field according to the reference system of the DEM simulation where the ship is moving and the water is still. The adaptation of the reference frame when converting the CFD flow field into DEM has to be done manually inside the flow field conversion module by a visual assessment of the CFD reference frame of the simulations done for ship and propeller. Therefore, the flow field conversion options are added for the actuator disk and the ship CFD simulations in this module where the flow fields are adjusted to the reference frame of the DEM simulation before the interpolation of the flow fields for the simplified (converted) grid for the DEM calculations.

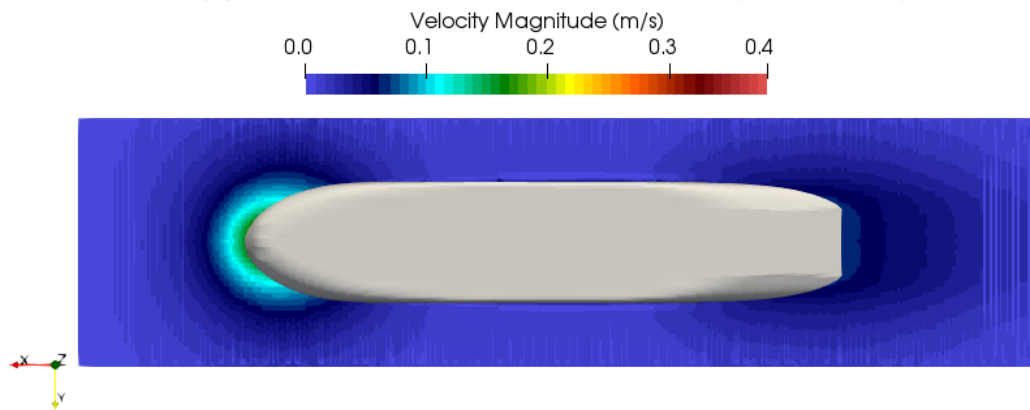
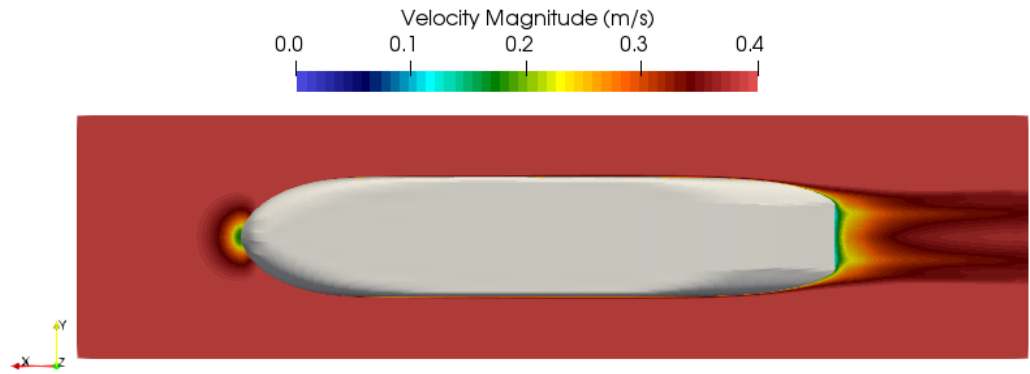


**Figure 47:** Comparison of ship velocity fields between the converted flow field and the CFD flow field (bottom views)

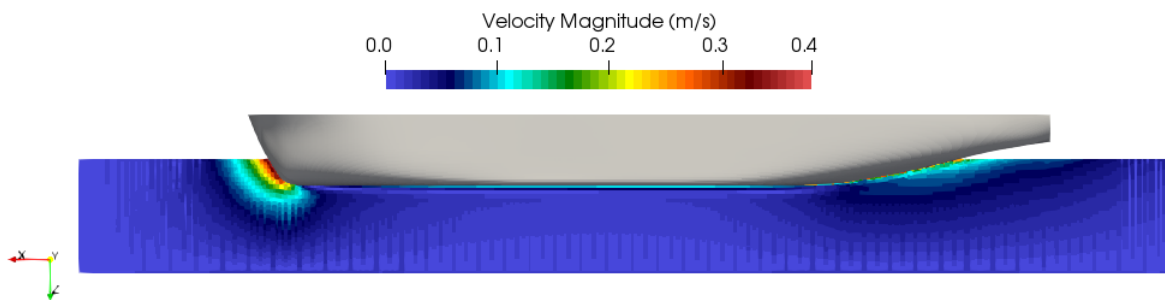
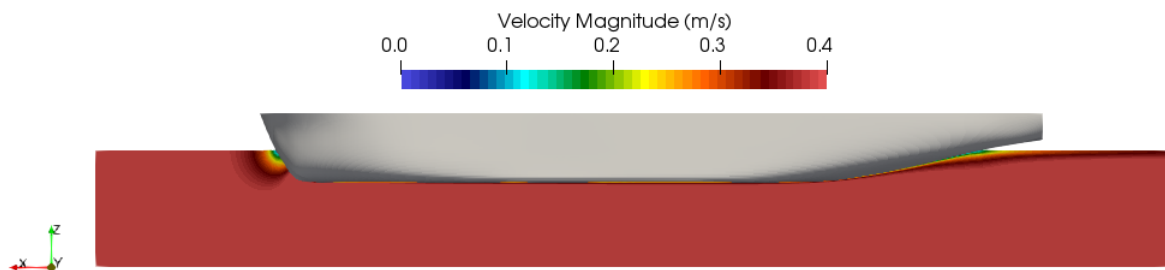


**Figure 48:** Comparison of ship velocity fields between the converted flow field and the CFD flow field (side views)

The tolerance value in the flow field conversion is taken the same as the actuator disk case ( $tol = 20mm$ ); however, the  $d_{gn}$  number is taken to be  $10mm$  in order for reducing the number of points in the newly generated grid; consequently reducing the computational burden. As a result, the quality of the converted flow field acquired is found to be a good approximation of the real CFD flow field of the ship, even though the converted (interpolated) flow field behind the ship is not in good agreement with the original CFD simulation (figure-47). To overcome this issue, the tolerance value can be increased in the flow field conversion simulation so as to increase the amount of found nodes, which is related to the quality of the new grid. All in all, the converted flow field is found to be good enough to proceed since acquiring a flow field with high accuracy is not the main scope of this study.

### **5.3.2.2 Model Ship Simulation In Brash Ice with the Improved Tool**

The brash ice model simulation with the improved tool will be carried out in this section. The triangulated mesh of the ship model is presented in the figure-49. The number of polygons is kept as small as possible in order to reduce the computation time. The skeg part of the ship was removed as explained earlier to avoid non-convex surfaces which is unwanted by the contact detection algorithm.

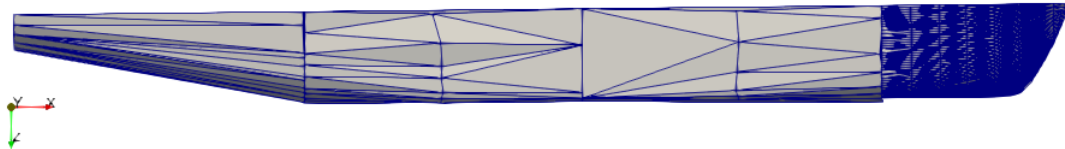


**Figure 49:** Triangulated ship mesh used in the brash ice model simulation

The basic configuration for the brash ice model simulation is presented in the figure-50. The simulations are done in ballast condition with the ship trims by the stern. There are three simulation cases created in order to make a comparative analysis: simulation with no flow field, simulation with multiple flow fields (ship and actuator disk flow fields), simulation with ship flow field, and simulation with actuator disk flow field. The actuator disk is positioned the same location as the location of the propeller in the real model.

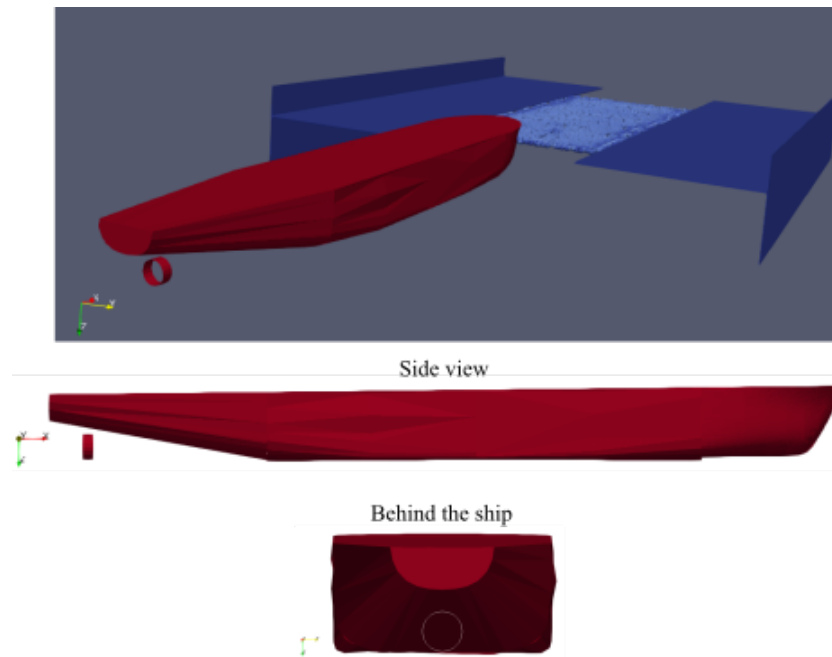
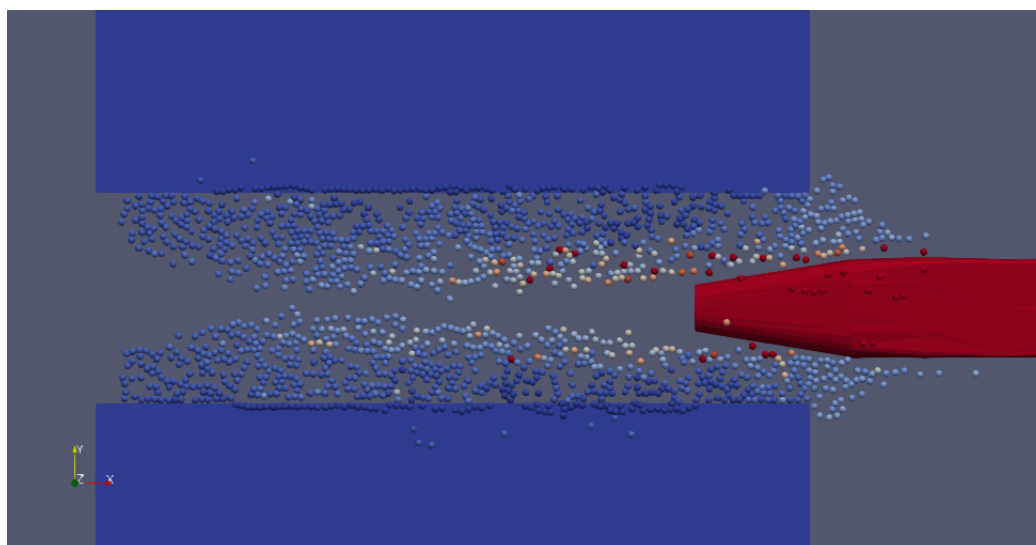
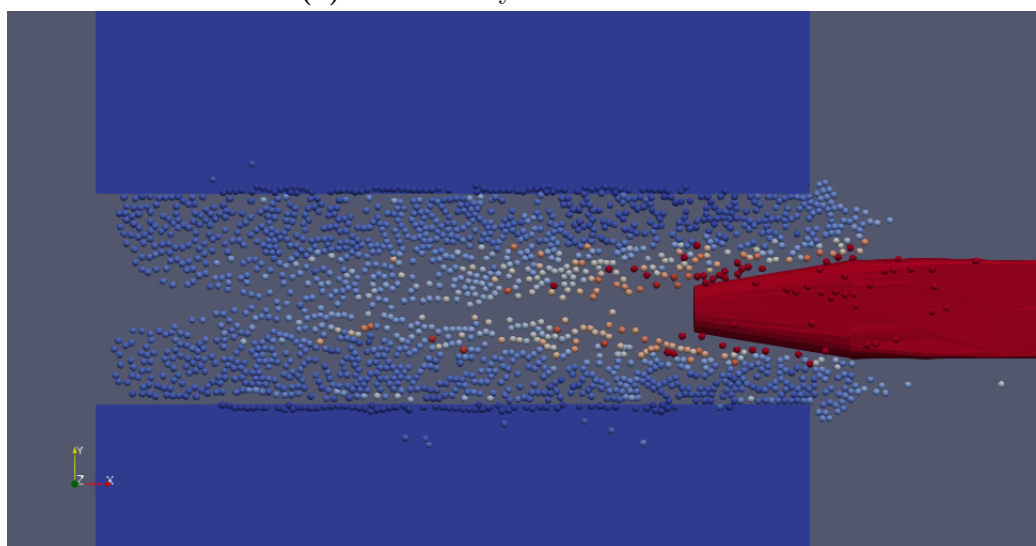


**Figure 50:** Brash ice model simulation configuration

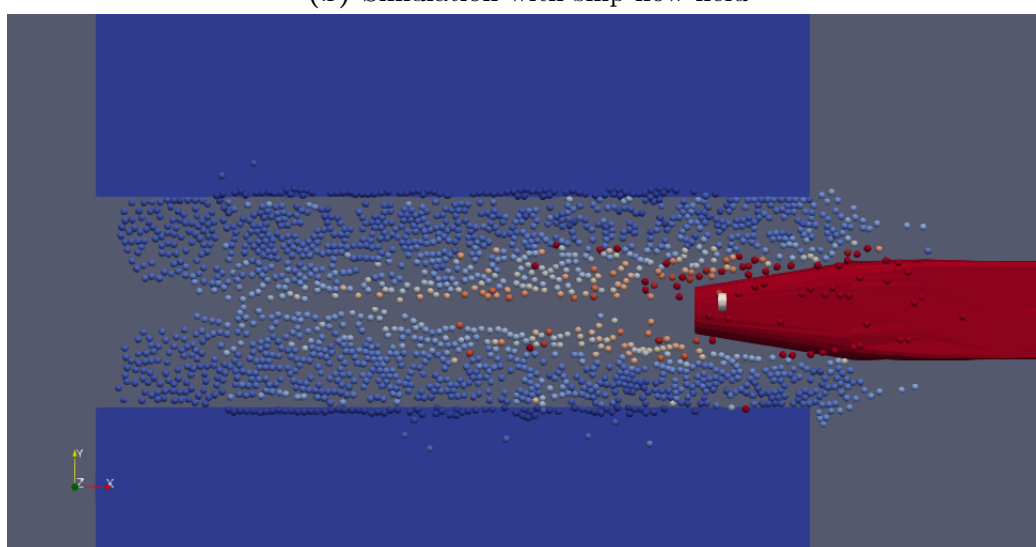
The visual comparison of the simulations from the bottom of the ship are provided in the figure-51. When comparing the figure-51b to the figure-51a, it can be seen that the flow field behind (wake) the ship causes the closing of brash ice particles when the ship passes through the channel which is more realistic and closer to the model test observations. The effect of the actuator disk can be observed in comparison between the figure-51b and figure-51c such that the channel behind the ship is more clear of the brash ice particles due to the flow field pushed by the actuator disk volume force. Detailed comparison is made between simulation with multiple flow field and no flow fields in the figure-52. The images are taken at the same time output. It can be seen from the figure at the top that the brash ice particles at the bow of the ship is pushed to the sides due to the effect of the ship flow field (the region inside the green area) in comparison with the the figure at the bottom (no flow field). Furthermore, in the simulation performed with multiple flow fields (top view in figure-52), the ship is moving faster (the simulation consists in a propulsion test where only the propeller RPM is fixed, but the speed is variable) than the ship situated in the simulation without flow fields (bottom view in figure-52). The distance between the ships in both simulation is shown in blue arrow in the figure-52. The reason is that the flow field insertion decreases the contact between the ship and the brash ice particles at the bow; consequently, reducing the brash ice resistance, and making the ship advance faster.



(a) Without any flow field insertion



(b) Simulation with ship flow field



(c) Simulation with multiple flow fields (actuator disk and ship)

**Figure 51:** Comparison of ship model brash ice simulations



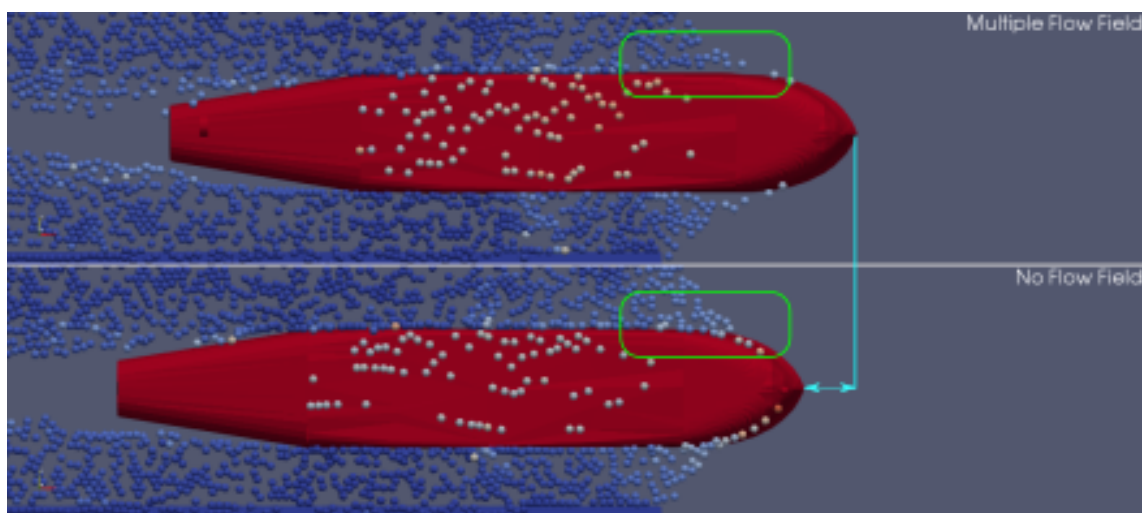


**Figure 52:** Detailed comparison of the simulations (multiple flow field vs no flow field)

The comparison with the experiment is also presented in the figure below. The underwater views from the aft for both simulation and experiment are compared. Although the channel openings seem to be similar for both the simulation and the experiment, in order to make a good judgement, the simulation must be run with sufficient brash ice thickness (at least 3-4 layers), and enough length of the brash ice channel (at least 1.5 times of the ship's length). However, in the time frame of this study, analysis couldn't be performed with the large amount of brash ice particles; since, it requires large computing resources that were not available for this study.

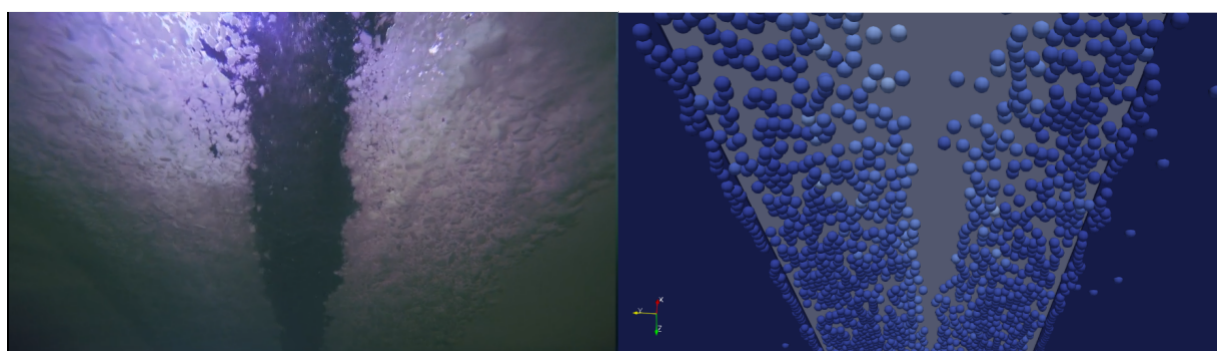


**Figure 53:** The underwater view of the channel behind the ship model for both experiment and simulation with multiple flow fields

## **6 Conclusion**

In this study, the hydrodynamics capability of the HSVA's brash ice simulation tool is improved in order to make multiple flow field insertion to the brash ice model simulation possible. For this purpose, the flow around the propeller is solved by modelling it as an actuator disk. After that, the actuator disk simulation case created is automatized in a way that it can be directly used from the DEM tool, and added as a new simulation type inside the DEM code. The automation process involves command line based user interface asking the user to enter the significant parameters of the propeller to start the CFD simulation, saving the required data output (velocity field) automatically without the need of opening ParaView GUI, and plotting the figures related to convergence history.

After automating the actuator disk simulation, the modified brash ice simulation tool is tested by a non-realistic cylinder-actuator disk setup. Three cases are compared to each other: the simulation with only single flow field (cylinder flow field), no flow field, and multiple flow fields (cylinder and two actuator disks). The results from these simulations verify that the improved tool is capable of performing the brash ice simulations with multiple flow fields.

Then, the improved tool is utilized on the brash ice ship model test simulation in order to observe the effect of the flow fields on the brash ice particles around the ship and behind the propeller. For that, the steady state, single phase (only water), incompressible RANS (Reynolds-averaged Navier–Stokes equations) based CFD simulation is performed to determine the flow around the ship. The three simulation cases are presented as follows: the brash ice ship model simulation with no flow field, single flow field (only flow around the ship), multiple flow fields (the ship and the actuator disk flow fields). As a result, it is observed that the flow fields inserted for the ship and actuator disk make a significant difference compared to the simulations done without any flow fields imported. It is also concluded that the ship flow field reduces the brash ice-ship contact at the bow, and it decreases the brash ice resistance, making the ship advance faster than the ship without any flow field.

Finally, the ship brash ice simulation with multiple flow fields is compared with the images from the ice model test. It is observed that there are many more brash ice particles and longer brash ice channel required to make a proper visual comparison.

## **7 Recommendations For Future Studies**

The future recommendations for further improvements of the brash ice simulation code are listed as follows:

- A real propeller can be modelled by taking into account its shape in order to have more accurate flow fields, and also to determine the forces arising from the contact between brash ice particles and the propeller.
- In the current status of the tool, the flow disturbance due to the brash ice particles' movement into the flow field is not considered. It should be taken into account to have a more realistic movement of the ice particles due to the hydrodynamic effect. However, it should be noted that this method (two way coupling) would require much higher CPU resources, since CFD simulation would need to be run during the time integration loop of the DEM code.
- The number of polygons of the ship imported into the tool is taken to be as few as possible to reduce the computation time. However, in order to have a realistic representation of the ship in the DEM simulation, an optimization can be carried out to determine the fewest number of polygons to define the ship geometry accurately.
- As mentioned before, the tool only allows for a qualitative assessment of the results. The code can be further improved in order to have accurate quantitative results (improving contact force algorithm, detailed validation of the flow fields obtained etc.).
- The brash ice simulations for the ship with multiple flow fields must be realized for large amount of brash ice particles in order to make a clearer qualitative assessment of the brash ice particle movement around the ship, and the brash ice channel opening behind the ship.

## References

- [1] K.Takamune and E.Robert. “Resistance To Ship-Hull Motion Through Brash Ice”. In: *Cold Regions Science and Technology* 10 (1984), pp. 219–234.
- [2] Ivan Montenegro Cabrera. “Smoothed particle hydrodynamics modeling of brash ice”. MA thesis. University of Rostock,EMSHIP/HSVA, 2017.
- [3] L.Wanszhen et al. “Numerical simulation of an ice-strengthened bulk carrier in brash ice channel”. In: *Ocean Engineering* 37 (2020). DOI: <https://doi.org/10.1016/j.oceaneng.2019.106830>.
- [4] Malith Prasanna. “Numerical Simulation of Brash Ice”. MA thesis. University of Rostock,EMSHIP/HSVA, 2018.
- [5] R. Kaj et al. “Modelling brash ice growth in ports”. In: *22<sup>nd</sup> IAHR International Symposium on Ice ,Singapore* (2014).
- [6] Finnish Maritime Administration. *Finnish-Swedish Ice Class Rule- The Structural Design and Engine Output Required of Ships For Navigation In Ice*. URL: [https://www.sjofartsverket.se/pages/40584/b100\\_1.pdf](https://www.sjofartsverket.se/pages/40584/b100_1.pdf).
- [7] Sazonov K.E. Dobrodeev A.A. “Ice resistance calculation method for a ship sailing via brash ice channel”. In: *Proceedings of the 25<sup>nd</sup> International Conference on Port and Ocean Engineering under Arctic Conditions, Delft, The Netherlands* (2019).
- [8] Konno A. et al. “Validation of Numerical Estimation of Brash Ice Channel Resistance With Model Test”. In: *Proceedings of the 22<sup>nd</sup> International Conference on Port and Ocean Engineering under Arctic Conditions, Finland* (2013).
- [9] M.Philipp. “Fully-Coupled CFD-DEM for Simulations of Ships Advancing Through Brash Ice”. In: *SNAME Maritime Convention, Tacoma, Washington, USA* (2019).
- [10] H. Luofent et al. “Simulation of a ship advancing in floating ice floes”. In: *SNAME Maritime Convention, Tacoma, Washington, USA* (2019).
- [11] Seo D.C. and Pallard R. “A Numerical Study of Interaction Between Ice Particles and Complex Ship Structures”. In: *Arctic Technology Conference, St. John’s, Newfoundland and Labrador* (2016).

- [12] Vroegrijk E. “Validation of CFD-DEM Against Measured Data”. In: *Proceedings of the ASME 2015 34<sup>th</sup> International Conference on Ocean, Offshore and Arctic Engineering, St. John's, Newfoundland, Canada* (2015).
- [13] Wang C. et al. “Analysis on ice resistance and ice response of ships sailing in brash ice”. In: *Chinese Journal of Ship Research, Harbin* 13 (2018), pp. 43–49. DOI: <https://doi.org/10.3969/j.issn.1673-3185.2018.01.011>.
- [14] Emily-Sophie Demmin. “Improvement of a Discrete Element Simulation of Ship Performance in Brash Ice”. MA thesis. Hochschule Bremen, 2020.
- [15] Strack O.D.L. Cundall P.A. “A discrete numerical model for granular assemblies”. In: *Géotechnique* 29.1 (2019), pp. 47–65.
- [16] Aleksei Alekseev. “Numerical Simulation of Ice Ridge Breaking”. MA thesis. University of Rostock, EMSHIP/HSVA, 2016.
- [17] Svenning E. *Implementation of an actuator disk in OpenFOAM*. Chalmers University of Technology, 2010.
- [18] Borna Šeb. “Numerical Characterisation Of A Ship Propeller”. MA thesis. University Of Zagreb, 2017.